MORPHOLOGY-DRIVEN SUPERHYDROPHOBIC POLYSTYRENE WEBS: FABRICATION AND CHARACTERIZATION

by

YUE YUAN

B.E., Wuhan Textile University, 2013

A THESIS

submitted in partial fulfillment of the requirements for the degree

MASTER OF SCIENCE

Department of Apparel, Textiles and Interior Design
College of Human Ecology

KANSAS STATE UNIVERSITY
Manhattan, Kansas

2016

Approved by:

Co-Major Professor
Jooyoun Kim

Approved by:

Co-Major Professor
Seong-O Choi

Copyright

Abstract

Superhydrophobicity (water contact angle, WCA >150˚) can be achieved by introducing surface roughness and decreasing surface energy. Polystyrene (PS) electrospun web can be used as an excellent substrate for superhydrophobic surface due to its low surface energy (~33 mN/m) and processibility to form various roughness. As the Cassie-Baxter model explains, the presence of roughness amplifies anti-wettability of materials whose surface energy is low (hydrophobic, WCA >90˚). This study aims to fabricate superhydrophobic PS nonwoven webs by electrospinning process and vapor deposition of 1H,1H,2H,2H-perfluorodecyltrichlorosilane (PFDTS) and to investigate the influence of fiber morphology and surface energy on wettability. To this end, PS webs with various fiber morphologies were electrospun under different polymer concentrations and solvent mixtures. PS substrates were treated by air plasma to attach –OH groups before the vapor deposition of PFDTS. Air plasma treatment itself increased the surface energy of PS; however, with PFDTS coating, the surface energy was decreased. The wettability was characterized by WCA and sliding angle measurement. WCAs on the electrospun webs were greater than that of flat PS film (WCA=95˚) due to the increased roughness of the web. The web with beads or grooved fibers achieved superhydrophobicity (WCA>150˚). PFDTS deposition lowered the surface energy of PS surface to about 15.8 mN/m. PS web with PFDTS deposition presented high water contact angle up to 169˚ and low sliding angle about 3˚. Also it was attempted to characterize the interfacial area between water and a solid surface on irregular fibrous webs. The fraction of solid surface area wet by the liquid (solid fraction) was observed by staining the rough electrospun web with a hydrophobic fluorescent dye, coumarin. The actual solid fraction corresponded fairly well with the theoretical solid fraction calculated by the

Cassie-Baxter equation, demonstrating that the treated superhydrophobic surface follows the Cassie-Baxter wetting state.

Table of Contents

List of Figures

List of Tables

Acknowledgements

This work is supported by 3M Non-Tenured Faculty Grant; University Small Research Grant (USRG) from the Kansas State University; and College of Human Ecology Sponsored Research Overhead Awards (CHE-SRO) from the Kansas State University. The author appreciates Dr. Daniel L. Boyle at the Microscopy Facility of Kansas State University for the help with fluorescence microscopy and Dr. Prem Thapa at the Microscopy and Analytical Imaging Laboratory of University of Kansas for the help with SEM.

Chapter 1 - Introduction

Surface wettability or anti-wettability is generally represented by a static contact angle (CA) and/or a sliding angle (SA, or roll-off angle). A surface with a water contact angle beyond 90˚ is a hydrophobic surface, while a hydrophilic surface has a water contact angle lower than 90˚. Furthermore, a surface with a high contact angle (typically >150˚) and a low roll-off angle (typically <10˚) is regarded as being super-repellent to the contacting liquid (Kota, Kwon, & Tuteja, 2014). With an emerging demand for super-repellent/superhydrophobic (super-repellent to water) textiles for potential applications in self-cleaning and protective textiles, there have been increasing efforts (Sas, Gorga, Joines, & Thoney, 2012) to produce super-repellent surfaces by various fabrication methods (Wolfs, Darmanin, & Guittard, 2013). In previous literature (Kota et al., 2014), fine roughness on surfaces and low surface free energy were determined as two crucial components for achieving super-repellency/superhydrophobicity (water contact angle, WCA >150˚).

Young's equation (Young, 1805) explains wettability by the relationship between the contact angle and the interfacial tensions among solid, liquid, and vapor (or air) phases for a flat surface. Thus, when a surface is flat and the vapor phase is air, the contact angle is solely dependent on the surface energies of solid and liquid phases. Low surface energy of a solid makes a hydrophobic surface, and high surface energy of a solid makes a hydrophilic surface. Later, Wenzel (1936) and Cassie-Baxter (1944) reported that hydrophobicity can be enhanced by introducing surface roughness on a hydrophobic flat surface.

Several literatures focused on the electrospinning technique as a fabrication method to create structural roughness for superhydrophobic surface design on low surface energy materials (Lin, Ding, & Yu, 2010; Miyauchi, Ding, & Shiratori, 2006). By adjusting controllable

parameters in the electrospinning process, various micro- or nanostructures can be built on electrospun web surfaces (Casper, Stephens, Tassi, Chase, & Rabolt, 2004; Huang, Zhang, Kotaki, & Ramakrishna, 2003). However, limited references exist on how specific roughness formed on a nonwoven surface affects repellent functionality. Previous studies reported different polymer fiber morphologies in electrospun webs regarding the evaporation rate of solvents (Zheng, He, Li, Xu, & Han, 2006); however, limited research focuses on the wettability of surface various from one specific fiber morphology to another.

In addition to forming surface roughness, modification of surface chemistry has been conducted as a critical process to achieve super-repellency; for instance, surface chemistry was modified to lower the surface energy by vapor coating processes (Kim, Kim, & Park, 2016; Shin, Lee, Moon, & Kim, 2012; Aulin, Netrval, Wågberg, & Lindström, 2010). Though the effects of surface roughness and surface chemistry (or surface energy) have been studied previously, little discussion has been made on the combined effect of electrospun-morphological parameters and surface energy. In this study, with an effort to investigate the combined effect of surface roughness and surface free energy on wettability, surface roughness and surface energy were controlled by the electrospinning process and air plasma/chemical vapor coating, respectively. The surface wettability was analyzed using theoretical models that explain surface wettability.

Commonly the wetting state of a super-repellent surface is explained by the Cassie-Baxter model (Cassie &Baxter, 1944). According to this model, the presence of roughness reduces the liquid-solid contacting area, enhancing anti-wettability. Previous studies attempted to predict the contact area between the water and rough surface (Kota et al., 2014; Kim et al., 2016); however, actual observation of the contact area between liquids and rough solids was not made. Especially, the irregular fibrous surface makes this observation more challenging.

The purpose of this study was to 1) fabricate super-repellent surfaces by electrospinning and vapor-coating processes; 2) investigate the relationship between surface morphology, surface free energy, and surface wettability (or repellency) and 3) develop a characterization method to have an actual measurement of the contact area between water and roughened solid. To this end, polystyrene (PS) that has low surface free energy (~33 mN/m) was used to produce super-repellent webs by the electrospinning and vapor-coating processes. The surface wettability was analyzed in terms of implemented surface roughness and surface free energy using the Cassie-Baxter model. To visualize the solid area that was in contact with water, fluorescence microscopy was used with a hydrophobic fluorescent dye, coumarin.

Research hypotheses

Electrospinning process

In order to fabricate electrospun webs with different roughness structures, electrospinning parameters were varied, including polymer concentration, mixing ratio of solvents, applied voltage, and feeding rate of polymer solution. Of particular interest was the effect of polymer concentration and solvent mixing ratio on the morphology of electrospun webs, which are thought to form micro- and nanoscale roughness on the webs. From the results, the relationship between the electrospinning processes and the resulting morphology of electrospun webs were identified, and the following two research hypotheses were tested:

Hypothesis 1: *in electrospinning, higher concentrations (above the critical point for chain entanglement) of polymer solution will produce uniform fibers, while lower concentrations (below the critical point for chain entanglement) of polymer solution will produce beads.*

Hypothesis 2: *a mixture of solvents with different volatilities will generate irregular surface morphology during electrospinning.*

Influence of surface roughness and surface energy on wettability

Theoretical models on smooth surface and rough surface claimed two crucial components to achieve super-repellent property on surfaces: surface roughness and low surface free energy. According to the Young's model (Young, 1805), where the wettability is predicted solely by the surface free energy without consideration of surface roughness, lowering the surface free energy decreases the wettability (increases the repellency). When it comes to the role of roughness, other theories (Cassie & Baxter, 1944; Wenzel, 1936) explain that the roughness amplifies the intrinsic wettability of materials. We tested those theoretical hypotheses as follows:

Hypothesis 3: *increased roughness on a hydrophobic surface will enhance the anti-wettability.*

Hypothesis 4: *increased roughness on a hydrophilic surface will enhance the wettability.*

Visual observation of solid area that is in contact with water

In the Cassie-Baxter model (Cassie & Baxter, 1944), a solid area fraction (*fs*) represents the contact area between water and the rough solid surface. In this study, we visually observed the solid area where the liquid is actually in contact with, by employing fluorescence microscopy with a hydrophobic fluorescent dye. The observation was made on surfaces with different levels of repellency.

Significance of the study

Electrospinning technique, with its potential as a scalable process, has been extensively studied as a means to produce nano to micro-scale fibers with tunable morphology. As the surface wettability can be mainly controlled by the surface energy and the surface roughness, electrospinning techniques can be utilized as an effective method to control the wettability by varying the surface roughness. In other words, surface roughness with various morphological

characteristics can be produced by adjusting the electrospinning process parameters. It is significant to study the process parameters of electrospinning to create surface morphology and apply this roughened surface to produce super-repellent surfaces.

Though theoretical models (Cassie & Baxter, 1944; Wenzel, 1936) are available to predict the wetting behavior of solid substrates by the surface energy and the surface roughness, such models were developed without specific consideration of fibrous solid materials. Thus, this study aims to apply these theoretical models to predict the wettability of electrospun webs, which are in porous structures. The conclusion of this study will contribute to better understanding of design parameters for superhydrophobic/super-repellent surfaces, such as how fiber morphology and surface energy affect the anti-wettability of a fibrous surface. Also, the characterization method developed for wetted surface area is very relevant at the moment, as there are no established methods so far. The direct observation of actual contact area between water and superhydrophobic solid surface would help understand the wetting state of the surface, and this will give insights on design strategy for superhydrophobic surfaces.

Definition of terms

Electrospinning- A process to produce nonwoven webs with fine fibers, by generating high voltage electric field between an extruder of polymer solution and a metal collector.

Morphology- The forms and shape of structures. In electrospun webs, morphology involves the shapes and sizes of fibers, beads and other structures formed on surface.

Contact Angle- The angle measured for a liquid droplet placed on a solid surface; angle between a liquid/solid interface and a tangential line of liquid/air interface (Young, 1805). It is a measure of surface wettability of a solid surface.

Roll-off angle, sliding angle- The critical tilted angle of a surface that allows liquid droplet begins to slide down (Miwa, Nakajima, Fujishima, Hashimoto, & Watanabe, 2000).

Self-cleaning- Referring to the property that material can be cleaned by water rinsing (Sas et al., 2012). From a surface with self-cleaning ability, water drops easily roll-off from the surface. This rolling water can adhere to dirt on the surface and roll off together. By this rolling action, dirt can be removed from the surface, and this phenomenon is called self-cleaning.

Surface free energy (surface energy, surface tension)- Intermolecular forces that are on the surface of a material. Larger surface energy means that intermolecular forces are strong within a material, and the material tends to form a shape with a minimized surface area. Surface tension is the identical term made to describe the liquid phase.

Plasma treatment- Gases are ionized through the high energy input and sustained by the radio frequency, leading to chemical and physical reactions with the sample surface.

Hydrophobic recovery- Referring to the phenomena that hydrophobicity of a surface hydrophlized by plasma treatment returns to its original hydrophobic state after aging time (Borcia, Anderson, & Brown, 2004).

Chemical vapor coating- Also known as chemical vapor deposition. It is a gas phase coating method, which allows the deposition of a monolayer of chemicals or formation of functional groups on the surface, thereby modifying the surface chemistry.

Solid fraction (*fs*)- In the Cassie-Baxter (Cassie & Baxter, 1944) wetting model, solid fraction refers to the fraction of the solid surface area wet by the liquid.

Chapter 2 - Literature review

Theories on surface wettability

Wettability of a solid is governed by the surface free energy (surface energy, or surface tension) of a material (Young, 1805) and the surface roughness resulting from surface morphology and topography (Cassie & Baxter, 1944; Wenzel, 1936).

Surface free energy

Wettability refers to the interaction between liquid and solid phases and is commonly defined by the contact angle of a liquid drop (or droplet) on a solid substrate (**Figure 2.1**). When wetting occurs, a liquid droplet contacts a solid surface to form three-phase contact lines; solid-liquid, liquid-vapor and solid-vapor contact lines at the equilibrium state. Assuming a smooth and homogenous surface, Young's Equation (Young, 1805) gives the quantitative description by relating the static contact angle to the interfacial tensions of three contact lines, which is described as:

$$\gamma_{LV} \cdot cos\theta^{Y} = \gamma_{SV} - \gamma_{SL}.$$

θ^{Y}: contact angle at a smooth surface

γ_{LV}: interfacial tension between the liquid droplet and vapor

γ_{SV}: interfacial tension between the solid and vapor

γ_{SL}: interfacial tension between the solid and liquid.

By common definition, a hydrophilic surface gives the static water contact angle smaller than 90˚, and a hydrophobic surface gives a static water contact angle larger than 90˚.

Figure 2.1 Wetting model on a smooth surface

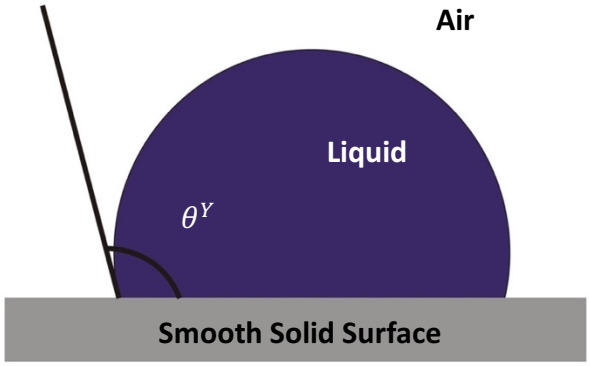

Young's Model

Surface roughness

While the Young's model applies only to a smooth surface without consideration of surface roughness, the Wenzel model (Wenzel, 1936) considers roughened surface by introducing the concept of "roughness factor," r, in the model. The Wenzel model can be written as:

$$cos\theta^W = r \cdot cos\theta^Y.$$

θ^W: apparent contact angle at the roughened surface in the Wenzel wetting state

θ^Y: contact angle on the smooth and homogenous surface in Young's equation

r: roughness factor, the ratio of the actual liquid-solid contact area on a rough surface to the projected contact area (**Figure 2.2a**).

In the Wenzel model, the roughness factor is always larger than unity, 1, because when a roughened surface is fully wet, the actual liquid-solid contact area is always equal (for a smooth surface) to or greater (for a roughened surface) than the projected contact area (**Figure 2.2 a**). The Wenzel model suggests that the roughness on a surface can enhance either hydrophobicity or

hydrophilicity, depending on the surface free energy of the material. In other words, if a solid material is hydrophilic with high surface free energy (when the water contact angle at a smooth surface is greater than 90˚), the presence of roughness enhances the hydrophilicity. If a solid material is hydrophobic with low surface free energy (when the water contact angle at a smooth surface is lower than 90˚), the presence of roughness enhances hydrophobicity.

Figure 2.2 Surface wetting models on rough surfaces

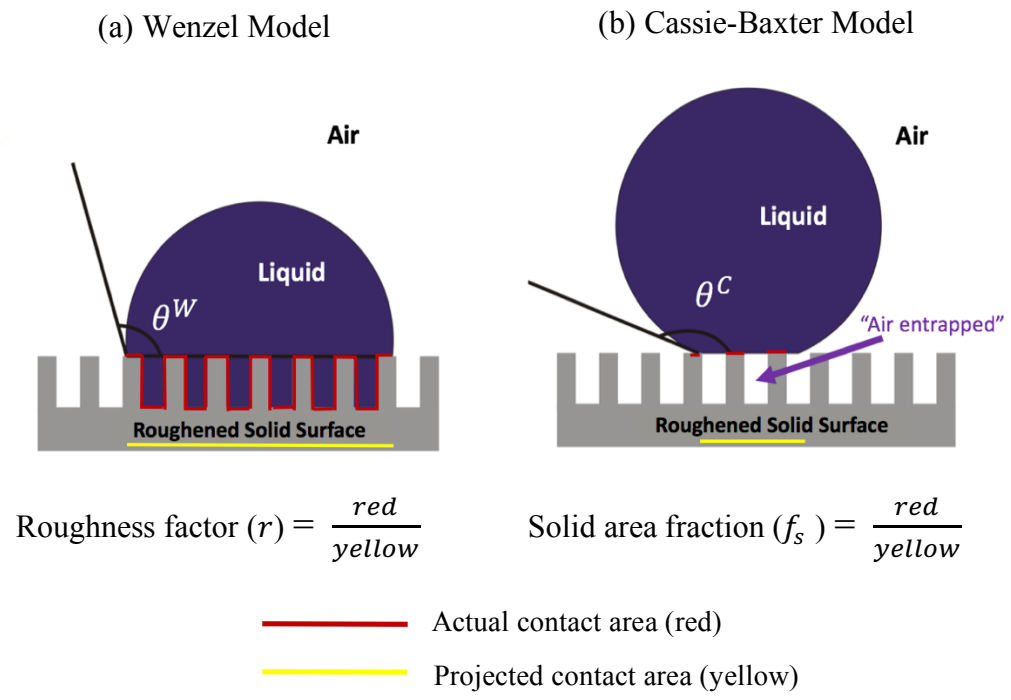

Another model that considers a roughened surface was suggested by Cassie and Baxter in 1944 (Cassie & Baxter, 1944). Compared to the all-wetting condition in the Wenzel model, the Cassie-Baxter model incorporates the air entrapped between the liquid and the roughened solid surface (**Figure 2.2b**). This model emphasizes the ratio of the contact area between liquid-vapor and that between liquid-solid. The solid area fraction, f_s, is defined as the ratio of the actual

solid-liquid contact area to the projected area (**Figure 2.2b**). The Cassie-Baxter model is given as the following:

$$cos\theta^C = f_s \cdot cos\theta^Y - f_v.$$

θ^C: apparent contact angle at the roughened surface in the Cassie-Baxter wetting state

θ^Y: contact angle on the smooth and homogenous surface in Young's equation

f_s: contact area fraction of liquid-solid interface

f_v: contact area fraction of liquid-vapor interface

Because of f_s+f_v=1, the model can be rewritten as the following equation to emphasize the solid area fraction only:

$$\cos\theta^C = f_s(\cos\theta^Y + 1) - 1.$$

In such a roughened surface, a liquid drop contacts the heterogeneous surface, generating liquid-solid interface and liquid-vapor interface. According to the model, reduction of solid-liquid contact area amplifies the apparent contact angle θ^C (**Figure 2.2b**). Previous study by Kota et al. (2014) experimented with this concept and reported that formation of roughness at a low surface energy surface increased the apparent contact angle, by minimizing the contact area between the liquid and solid (f_s) and increasing the contact area between the liquid and air (f_v).

A superhydrophobic surface (surface repellent to water) is generally defined to possess a static water contact angle above 150˚ with a small roll-off angle (usually lower than 10˚) (Wang & Jiang, 2007). As the surface becomes more repellent, the roll-off angle tends to become smaller. This roll-off angle is often associated with the self-cleaning ability of the repellent surface, where the rolling liquid drops can remove dirt on a surface while they roll off with the adhered dirt (Sas et al., 2012). Between the Wenzel state and the Cassie-Baxter state, the Cassie-

Baxter state is regarded as being more favorable to roll off the liquid drop from the surface, because the entrapped air reduces the contact area between the liquid and solid (f_s). Beside those models, there are transitional wetting states, which is in between the Wenzel and the Cassie-Baxter. In the transitional state, a liquid is partially penetrating through the roughness and in contact with and air (**Figure 2.3**).

Figure 2.3 Transition wetting state on roughened surface

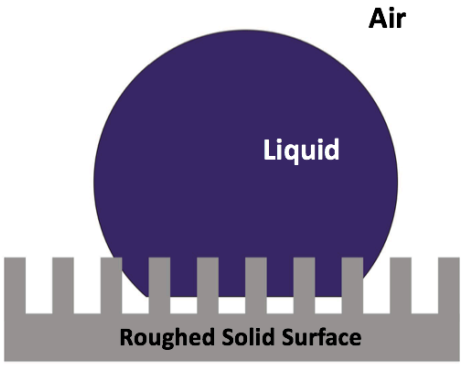

Transition Wetting State

In addition to measuring the contact angle of water (surface tension 72.8 mN/m at 20℃), several studies used other liquids with lower surface tensions, such as organic solvent and oil, to examine the oil-repellency or oleophobicity of surfaces. If the contact angle of an oily liquid is above 150˚, the surface is regarded as superoleophobic (Kota et al., 2014). The term "super-repellency" was used to explain the repellency or anti-wettability against water and other liquids in lower surface tensions. In this study, the term "super-repellency" was used interchangeably with "superhydrophobic" when the test liquid was water.

Fabrication of superhydrophobic surfaces

Fabrication of superhydrophobic/super-repellent surfaces have been extensively studied (Sas et al., 2012; Wolfs et al., 2013) since the hierarchical rough structure on a waxy material was observed on the natural superhydrophobic lotus leaf (Neinhuis & Barthlott, 1997). Since then, much researches followed to fabricate superhydrophobic surfaces that mimic such a surface structure (Wolfs et al., 2013) and to support the broad applications of superhydrophobic materials in protective equipment, self-cleaning materials and repellent textiles (Sas et al., 2012). The main design strategy for a superhydrophobic surface is to decrease the surface energy and to increase the surface roughness (Sas et al., 2012; Kota et al., 2014; Teare et al., 2002).

Surface energy modification

In order to achieve superhydrophobicity, the surface energy of a material needs to be reduced (Shafrin & Zisman, 1960). Surface energy modification can be achieved by the physical deposition or chemical bonding of chemicals in different surface free energies (Wolfs et al., 2013). Various physical and/or chemical processes have been applied to deposit or attach compounds with low surface energy, such as fluorinated compounds and silanes. Vice versa, surface wettability can be enhanced by increasing the surface free energy of the material by attaching high surface energy materials or by oxidizing the surface.

Increase of surface free energy

Gases are ionized in the plasma state, leading to chemical and physical reactions with substrate. Depending on the gases being used during the plasma process, it could either increase or decrease the surface free energy. Oxygen plasma can create functional groups such as hydrophilic hydroxyl (–OH) or carboxylic (–COOH) groups, increasing the surface free energy of the treated materials; the increase of surface free energy will result in the increase of surface

wettability. Shin et al. (2012) reported that polyethyleneterephthalate (PET) (with surface energy ~44.6 mN/m) nonwoven textile was modified to be hydrophilic after 60 minutes' oxygen plasma treatment. Similar results were reported for various polymers (Kim et al., 2016; Yoon, Moon, Lyoo, Lee, & Park, 2009). Longer treatment of oxygen plasma can cause redeposition of materials, giving a roughened surface (Kim et al., 2016).

Other than oxygen plasma, air plasma can be done without any additional gas set up to increase polymer surface energy; the oxidation utilizes the oxygen component of the air. Thereby, air plasma treatment can also increase the surface energy. Previous study reported that air plasma treatment changed the surface polarity, increased the oxygen ratio (Leroux, Campagne, Perwuelz, & Gengembre, 2009), and enhanced the hydrophilicity of the material. This air and oxygen plasma treatments can also be applied as a pre-step for later coating procedure by attaching functional groups to the surface that will facilitate the further chemical bonding in the coating process (Kim et al., 2016; Pan, Shahsavan, Zhang, Yang, & Zhao, 2015).

Decrease of surface free energy

The plasma processes can also be used to decrease the surface energy of materials, by coating the surface with compounds with low surface free energy. This process is referred to as plasma enhanced vapor deposition (PECVD). Commonly used monomers in this plasma process include fluorinated compounds such as CF_4 (Yoon et al., 2009; Woodward, Schofield, Roucoules, & Badyal, 2003) and silane compounds (Pan et al., 2015). As a type of silane compound, hexamethyldisiloxane (HMDSO) was deposited via PECVD in Kim et al.'s (2016) study to decrease the surface free energy of nylon and olefin polymers. The same procedure was utilized in Shin et al.'s (2012) study, generating a 20 nm thick SiO_x –C:H monolayer on a PET nonwoven textile surface to give the water contact angle above 160˚.

In addition, a vapor coating process can be done in vacuum conditions or in high temperature conditions to create a thin layer of coating with low surface energy compounds. Due to its very low surface tension, 1H,1H,2H,2H-prefluorodecylyerichlorosilane (PFDTS) has been used to make super-repellent surfaces (Aulin et al., 2010). Pan et al. (2015) treated the pillar-like, rough polydimethylsiloxane (PDMS) surface with PFDTS, and formed $–CF_3$ coating layer on the material, achieving superhydrophobicity. In another study, dodecyltrimethoxysilane (DTMS) was treated on cotton fabrics by the vapor coating process, producing a superhydrophobic surface with the water contact angle up to 156˚ (Ding et al., 2006).

Beside the vapor coating method, dip-coating has been applied as a common and simple procedure. Huang, Wen, Cheng, & Yang (2012) developed a superhydrophobic nonwoven paper filter by immersing the paper in a fluorinated waterborne epoxy emulsion, and the resulting material reached the water contact angle of 152˚. Fluorinated compounds are often favored to reduce the surface free energy in the coating procedure to achieve superhydrophobicity. In Xue, Jia, Zhang, & Tian' (2009) study, PFDTS was applied to a cotton textile by the dipping method, and the resulting fabric reached the water contact angle of 170˚ and an extremely low roll-off angle of 3˚.

Surface roughness modification

Forming roughness on surfaces is preferred or necessary to produce superhydrophobic/super-repellent surfaces (Cassie & Baxter, 1944; Sas et al. 2012; Wenzel, 1936). Previous research has introduced many techniques for generating micro- and/or nanoscale surface roughness in fabricating super-repellent surfaces; these methods include electrospinning, etching surfaces, and attaching nanoparticles on surfaces (Sas et al., 2012). Various morphologies of roughness were created on surfaces in previous studies, such as micro- or

nanoscale pillars (Kim et al., 2016; Pan et al., 2015) and irregular fibrous structures (Sas et al., 2012; Wolfs et al., 2013).

Plasma etching

Inductively coupled plasma reactive ion etching (ICP-RIE) can also create nanostructures on a surface by the physical etching of substrates. Oxygen plasma with high energy has been utilized in prior research as a means to forming nanoscale pillar-like structures; the created roughened structure was applied to produce super-repellent surfaces (Kim et al., 2016; Shin et al., 2012). PET nonwoven textiles with "nanopillars" on fibers exhibited the high water contact angle of 160˚ after 60 minutes' oxygen plasma etching followed by a PECVD procedure of HMDSO (Shin et al. 2012). From the study by Kim et al. (2016), a longer etching time contributed to forming the nanopillars in higher aspect ratio, increasing the surface roughness of the treated materials. Although oxygen plasma treatment can generate roughened surfaces that help achieve superhydrophobicity, surface energy will also be increased due to the simultaneous surface oxidation, adversely affecting superhydrophobicity. Thus, an extra step of surface modification is required to lower the surface energy of materials if plasma etching was performed using oxygen gas (Kim et al., 2016; Shin et al., 2012).

Electrospinning

Electrospinning has been used to create roughened surfaces by controlling the electrospinning parameters such as an applied voltage, solution concentration, and feeding rate of polymer solution. Super-repellency can be achieved by electrospinning alone without further introduction of roughness, if 1) a hydrophobic polymer is used as substrate, and 2) a favorable roughness structure can be created through the electrospinning process. More literature will be

reviewed in a separate section on the electrospinning apparatus, electrospinning procedures, and electrospinning application in super-repellent surface fabrication.

Electrospinning

Electrospinning has become well known as an effective process to produce continuous nanofibers from polymer solutions or melted polymers in the recent decade. The diameter of fibers in electrospun webs can be varied from micrometers to nanometers. Because of its very large surface-to-volume ratio (Huang et al., 2003), electrospun webs have been used as substrates for functional membranes and textiles to be applied as protective surfaces, filters, and tissue scaffolds (Bognitzki et al., 2001; Sas et al., 2012).

In general, an electrospinning apparatus consists of three components: a solution feeding part, a conductive collector, and a high voltage supply (Huang et al., 2003), as shown in **Figure 2.4**. During electrospinning, electrostatic force allows to form a jet of polymer solution from the tip of a needle (Reneker & Chun, 1996). The movement of a polymer solution between the needle and collector elongates the jet to become extremely thin. In the meantime, the evaporation of the solvent leaves the polymer fibers on the collector (Doshi & Reneker, 1993). Critical electrospinning parameters such as the viscosity, conductivity and surface tension of the polymer solution and the applied voltage have been studied in literature (Fong, Chun, & Reneker, 1999; Reneker & Chun, 1996). These parameters not only affect the process of electrospinning but also contribute to various fiber morphologies within the electrospun webs.

Figure 2.4 Electrospinning equipment

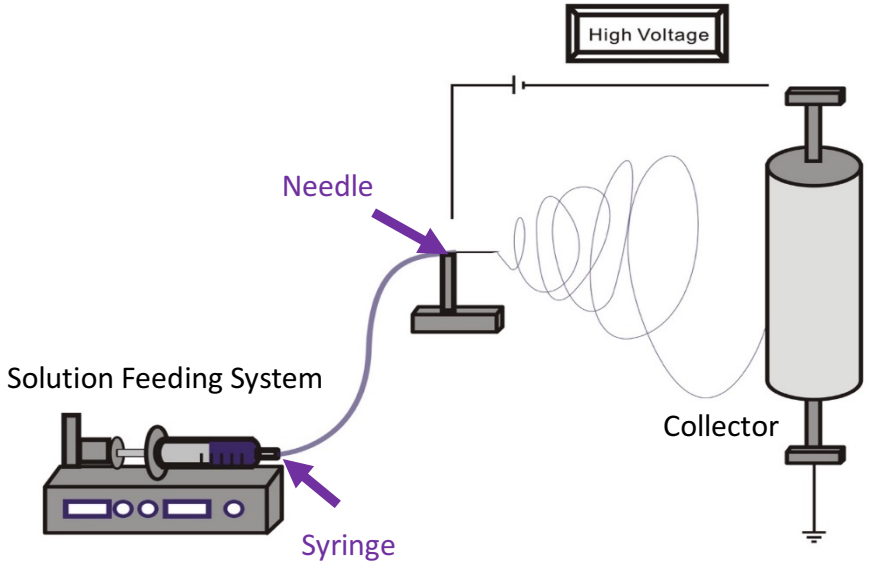

In electrospinning, uniform fibers and beaded fibers are often two typical fiber morphologies (Fong et al., 1999). General rules can be concluded from literature that relatively high polymer concentration (Lin et al., 2010; Miyauchi et al., 2006) and low applied voltage are preferred in forming smooth uniform fibers, while relatively higher applied voltage and low polymer concentration contribute to a beaded structure (**Figure 2.5**). Some literature has also attributed the formation of a beaded structure to the capillary breakup of the jet caused by surface tension (Fong et al., 1999), resulting in failure to maintain the polymer solution jet in the electrical field. In addition, the size or diameter of the fiber has been investigated in previous research as one respect of the electrospinning parameters-related fiber morphology. In general, high concentrations of a polymer solution contribute to larger fiber diameters; Lin et al. (2010) produced micrometer-range PS fibers with 30 wt% polymer concentration and nanofibers in 50 nm diameter with 5 wt% PS solution (Zheng et al.,2006).

Figure 2.5 FE-SEM images of PS electrospun webs with different solution concentrations (Lin et al. 2010)

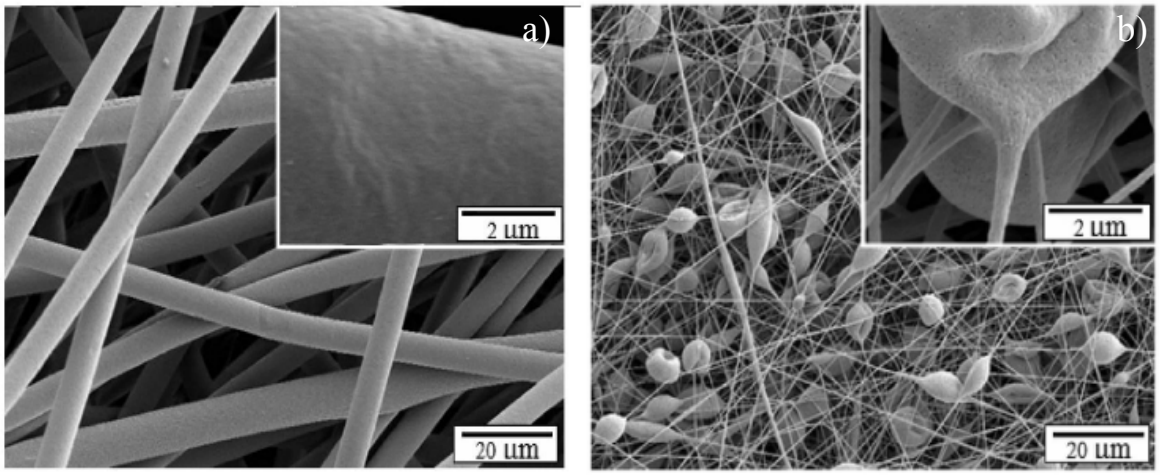

a) uniform fibers with 30 wt% PS in 1:3 (THF/DMF) solvent, larger fiber diameters, b) beaded fibers with 10 wt% PS in 1:3 (THF/DMF) solvent, smaller fiber diameters

In addition to the uniform fibers and the beaded fibers, other fiber morphologies have been reported. Megelski, Stephens, Chase, & Rabolt (2002) produced porous fibers from polycarbonate (PC), polystyrene (PS) and poly (methyl methacrylate) (PMMA) by dissolving them in chloroform ($CHCl_3$), tetrahydrofuran (THF), and acetone. The pores' diameters ranged from 50 to 1000 nm. Bognitzki et al. (2001) and Lin et al. (2010) explained that porous fibers are formed by the rapid evaporation of the solvent.

Electrospinning can be used as an effective procedure for fabricating surface roughness, such as fibers and beads, to make superhydrophobic surfaces (Ding et al, 2006; Sas et al., 2010; Yoon et al., 2009). Electrospinning with low surface-energy polymers, such as fluorinated compounds, may directly produce superhydrophobic surfaces. Zhu, Zuo, Yu, Yang, & Cheng (2006) generated "pop-corn" like beaded structures with poly (hydroxybutyrate-co-

hydroxyvalerate) (PHBV) via the electrospinning process, resulting in the water contact angle of 158°.

The morphology of electrospun webs has been related to the level of repellency. Although beaded structures were intially considered as by-products in the electrospinning process at first (Fong et al., 1999; Zhu et al., 2006), researchers found that beaded structures are preferred to achieve higher surface repellency compared to the uniform fiber morphology (Sas et al., 2012). When electrospun webs with micro-beads were produced using a fluorinated polymer blend, the contact angle of heptane (surface tension ~ 20.1 mN/m) was above 150°, showing superoleophobic properties (repellent to low surface tension liquid).

Because PS has relatively low surface energy (~33 mN/m), the superhydrophobic surface can be designed on a PS electrospun web by only generating micro- and/or nanoscale surface roughness via electrospinning (Kang, Jung, Kim, & Jin, 2008; Sas et al., 2012). When complex fiber morphology with porous structures or wrinkle fibers was produced, the resulting surface showed the water contact angle of up to162°. For PS polymer solution, solvents N, N-dimethlformamide (DMF) and THF are often used (Jarusuwannapoom et al., 2005). By adjusting the mixing ratio of solvents with different vapor pressure, PS electrospun fiber morphology can be varied (**Figure 2.6**).

Figure 2.6 PS Electrospun web morphologies

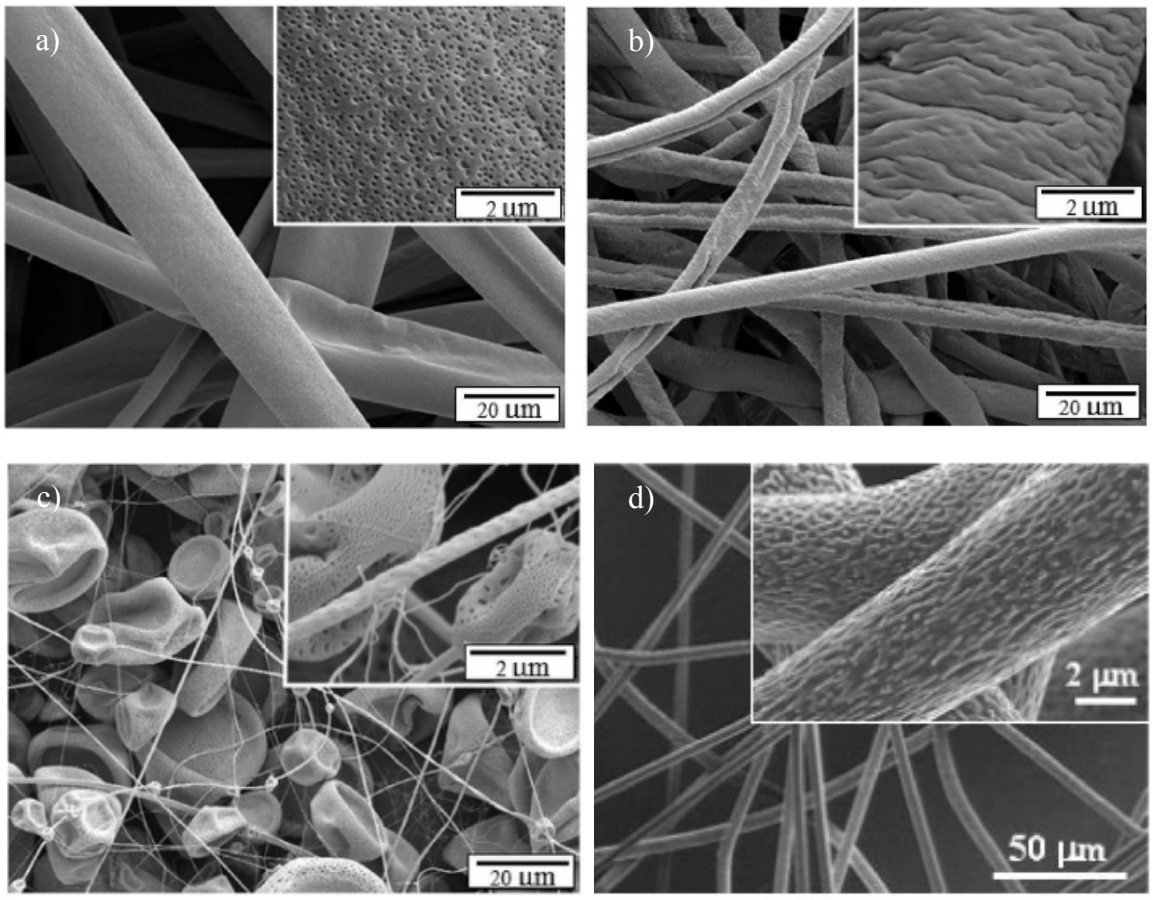

a) porous uniform PS fiber (THF: DMF=4:0), b) wrinkle uniform PS fiber (THF: DMF=3:1), c) porous beaded PS fiber (THF: DMF=4:0) (Lin et al. 2010), d) uniform PS fiber with another topology (THF: DMF=1:3) (Miyauchi et al., 2006).

Estimation of contact area between water and superhydrophobic surface

According to the Cassie-Baxter equation (Cassie & Baxter, 1944), the contact angle is increased as the fraction of the contact area between liquid and solid (solid fraction, f_s, **Figure 2.2 b**) is reduced. Knowing that the solid fraction f_s is a factor that explains the surface wettability in the Cassie-Baxter model (Cassie & Baxter, 1944), efforts have been made to estimate the solid fraction (f_s), mostly by measuring the geometric dimensions of rough structures. In Park, Park, & Kim's (2014) study, the upper surface area of nano-pillars formed on a superhydrophobic substrate was estimated, and the area fraction of the upper surface was used as the estimate of solid fraction, f_s. However, it is not a true representation of the surface area that the liquid is in contact with, and little evidence was provided whether this geometric estimate of roughness is truly represented as f_s. Kwon et al. (2014) observed water droplets on a superhydrophobic fabric surface by an environmental scanning microscope (ESEM); however, the resolution of ESEM was not high enough to observe the contacting interface between water and the fabric surface. Also, the water droplets on the surface were not stably positioned; they rolled off the surface during the ESEM observation.

Often a low roll-off (or sliding) angle is suggested as an indirect evidence of the Cassie-Baxter's wetting state (Cassie & Baxter, 1944) where a liquid is held by the entrapped air, thereby allowing an easy roll-off (Sas et al., 2012). In this wetting state, the uppermost area of a roughened substrate would be a close estimate of the contact area between the liquid and solid, which is f_s. A characterization method that enables the direct observation of solid wetting area would help better understanding of wetting phenomena and design strategy for super-repellent textiles.

Chapter 3 - Methodology and experiments

Figure 3.1 Schematic of overall approach

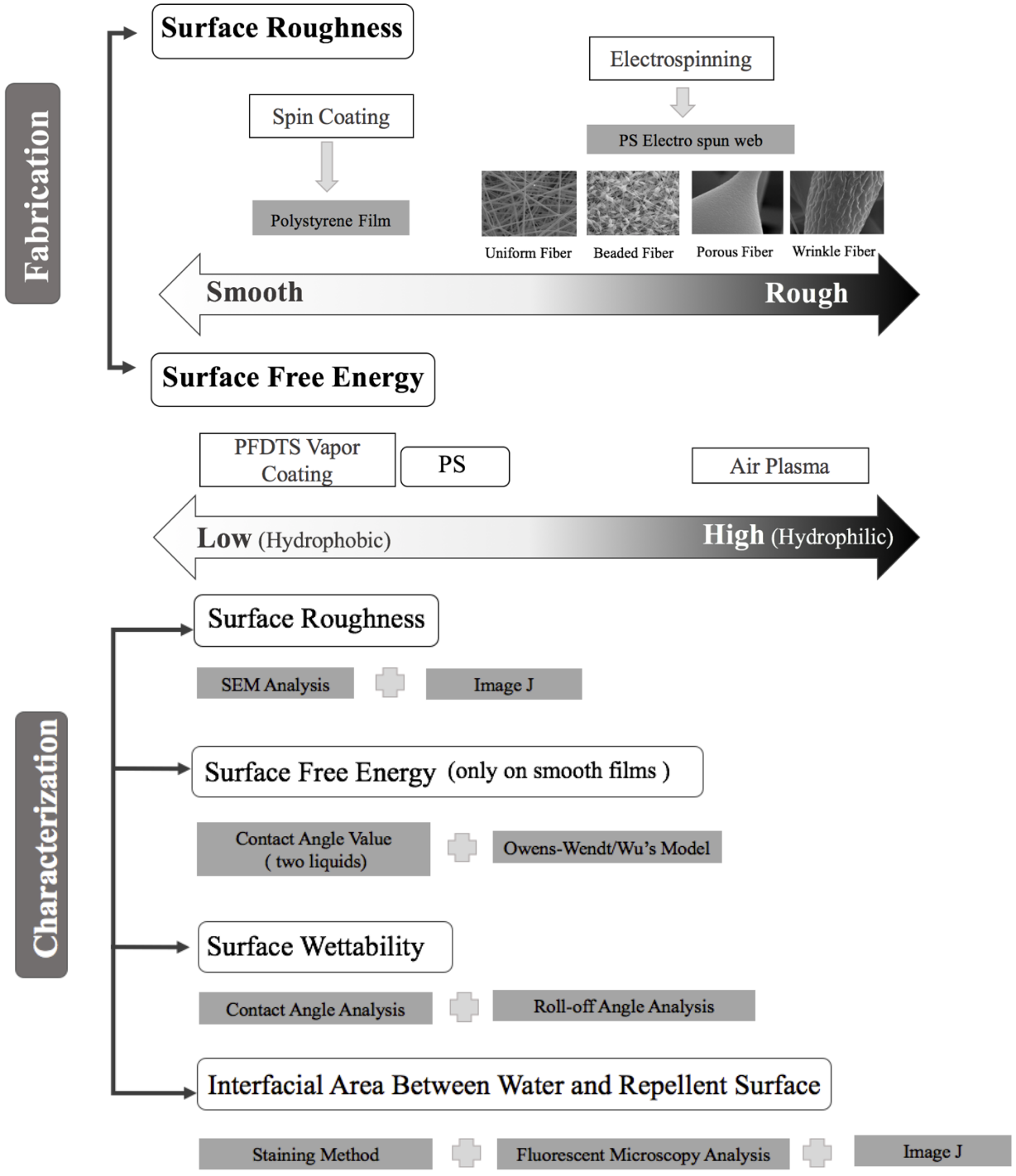

Overview of methodology

This study was conducted in multiple phases including fabrication of material, characterization of material, and theoretical analysis on material characteristics. The schematic of overall approach is shown in **Figure 3.1**.

Superhydrophobic polystyrene (PS) nonwovens were fabricated by forming surface roughness and reducing the surface energy. Micro- and/or nanoscale roughness was introduced via the electrospinning process by adjusting the electrospinning conditions. To investigate the effect of surface roughness on wettability, surfaces bearing different morphologies were created: smooth PS film by spin coating and PS electrospun fiber webs with various geometries such as beaded fibers, wrinkled fibers, and smooth fibers.

To investigate the influence of surface energy on wettability, the surface free energy of PS surfaces was modified by surface oxidation and/or vapor coating. To make the surface hydrophilic (increase of surface free energy), air plasma process was conducted for surface oxidation. To make the surface more hydrophobic (decrease of surface free energy), 1H,1H,2H,2H-perfluorodecyltrichlorosilane (PFDTS) was deposited onto PS surfaces in a vapor phase.

Surface wettability was examined by the static contact angle of water and methylene iodide (MI). The influence of surface free energy and surface roughness on wettability or repellency was investigated by characterizing the surface morphologies, surface energy and wettability of materials. Surface morphology of the smooth film and electrospun fibers was analyzed from SEM images using ImageJ software (version 1.46r, NIH, USA). Surface energy of the materials (untreated PS, air plasma-treated PS, vapor-coated PS) was calculated by putting

the contact angle measurement data of water and MI into the Owens-Wendt model and Wu's model.

To analyze the influence of surface roughness on the wetting characteristics, it was attempted to visually observe the fraction of the PS surface area which is in contact with liquid by employing fluorescence microscopy with a hydrophobic fluorescent dye, coumarin. In order to examine the validity of the developed characterization method, the solid fraction observed by fluorescence microscopy was compared with the theoretical solid fraction calculated by the Cassie-Baxter wetting model.

Fabrication of superhydrophobic PS surfaces

Material

Polystyrene (PS) with the weight-average molecular weight (Mw) of 192,000 g/mol was purchased from Sigma-Aldrich (USA). N, N-dimethlformamide (DMF), tetrahydrofuran (THF) and toluene, all in ACS grade, were purchased from Sigma-Aldrich (USA) and were used as received. 1H,1H,2H,2H-perfluorodecyltrichlorosilane (PFDTS) (96%) was purchased from Alfa Aesar (USA).

Spin coating

PS film with a thin, smooth surface was prepared by spin coating on a 2 cm×4 cm glass slide, which was pre-cleaned by acetone, isopropanol and deionized water in sequence, using a spin coater (VTC-100, MTI Corporation, USA). PS pellets were dissolved in toluene at 12 wt% concentration, and a glass slide was covered with 1.2 mL of the PS solution until the whole surface was covered. Thin PS film was then formed by spin coating at 2000 rpm for 60 seconds; the spin speed was ramped from 500 rpm to 2000 rpm for 2 seconds. The spin coated films were placed on a hotplate at 110°C (above 100°C, the glass transition temperature of PS) for an hour

to further remove the solvent. The spin coated smooth PS film were used as the control sample for comparison with the surface roughness of the electrospun webs. Surface energy before and after the surface modification (plasma treatment and/or chemical vapor coating) was calculated from the measured contact angles of the PS films.

Electrospinning

Electrospinning was used as a process to generate various micro- and/or nanoscale roughness of PS surface, thereby achieving the superhydrophobic/super-repellent surfaces. An electrospinning setup composed of a high power source, drum type collector, and syringe pump was purchased from Spraybase® (USA). A polystyrene solution was filled in a 10 mL syringe (Fisher Scientific, USA), and a polytetrafluoroethylene (PTFE) tubing (Kinesis, USA) was used to connect the syringe to a syringe pump. The other edge of the tubing was connected to a hypodermic needle, which was connected to the high voltage source. A grounded aluminum cylinder collector was placed in front of the needle as a target for collecting electrospun webs.

PS solutions of different concentrations (10, 20, and 30 % w/w) were prepared in a mixture of THF (vapor pressure of 19,065 Pa) and DMF (vapor pressure of 516 Pa) with different volume ratios. About 5~9 mL of the polymer solution was fed into a 10 mL syringe with a 22-gauge needle (inner diameter of 0.41 mm and outer diameter of 0.72 mm). The polymer solution was ejected by the syringe pump at feeding rates ranging from 1-2 mL/hr to optimize the electrospun conditions.

As a collecting substrate, a parchment paper (Wilton, USA) was wrapped on the metal drum-type collector for easier separation of the collected electrospun web from the collecting substrate. The rotating speed of the drum collector was kept at 100 rpm, and the distance between the needle and collector was fixed at 10 cm in order to optimize other process

parameters. The voltage applied to the needle ranged from 7 kV to 14 kV to generate the "Taylor cone" of the polymer solution at the needle tip. The Taylor cone formation at different flow rate was examined for the optimization of the electrospinning process. All the electrospinning experiments were conducted at room temperature with 45± 5% humidity. The electrospun specimen was placed in the fume hood for 3 hours at room temperature to evaporate the remaining solvent.

Plasma process

The purpose of air plasma treatment in this study is to add hydrophilic functional groups that offer the bonding sites for PFDTS chemical. However, before treating with PFDTS, hydrophilic functional groups created on PS surface increases the surface energy, enhancing the surface wettability. The influence of increased surface energy (by air plasma) combined with the presence of surface roughness on surface wettability was analyzed.

For the air plasma treatment, PS spin-coated film and electrospun webs were placed into the cylinder chamber of the air plasma equipment (PDC-32G, Harrick Plasma, USA). The pressure of the chamber during the air plasma treatment was kept constant at 100 mTorr, and the RF power of 18 W was applied for 3 min. Through this treatment, the carbon hydrogen bond (C-H) of PS were oxidized, thereby producing more hydrophilic -OH and -COOH groups on PS surfaces. In order to prevent the hydrophobic recovery of the plasma-treated substrates, samples were vapor coated within 1 hr or kept in distilled water immediately after the plasma treatment, and dried for 1 hr prior to further analysis or process.

Vapor coating

To decrease the surface energy of PS substrates, PFDTS (surface energy of 17.2 mN/m) was deposited by a vapor coating process on the plasma-treated PS substrates. Prior to the vapor-

coating, -OH groups were attached on the PS surfaces to facilitate the chemical bonding with PFDTS. 0.5 mL of PFDTS was diluted to 5% (v/v) in hexane, then 5 mL of diluted solution was pipetted into a petri dish that is placed in a glass vacuum desiccator. PS samples was hung on a copper wire frame, which was placed in the desiccator (**Figure 3.2**). The pressure inside the desiccator was lowered to approximately 100 Torr by using a vacuum pump. The desiccator was kept at room temperature for 1 hr followed by being placed in an oven at 70 °C for 1 hr. Chemical compositions of the PS substrates after the air plasma treatment and PFDTS vapor coating were analyzed by Cary 630 FTIR-ATR spectrometer (Agilent Technologies, USA). Specimen codes for different substrates and treatments are shown in **Table 3.1**.

Figure 3.2 PFDTS vapor coating apparatus

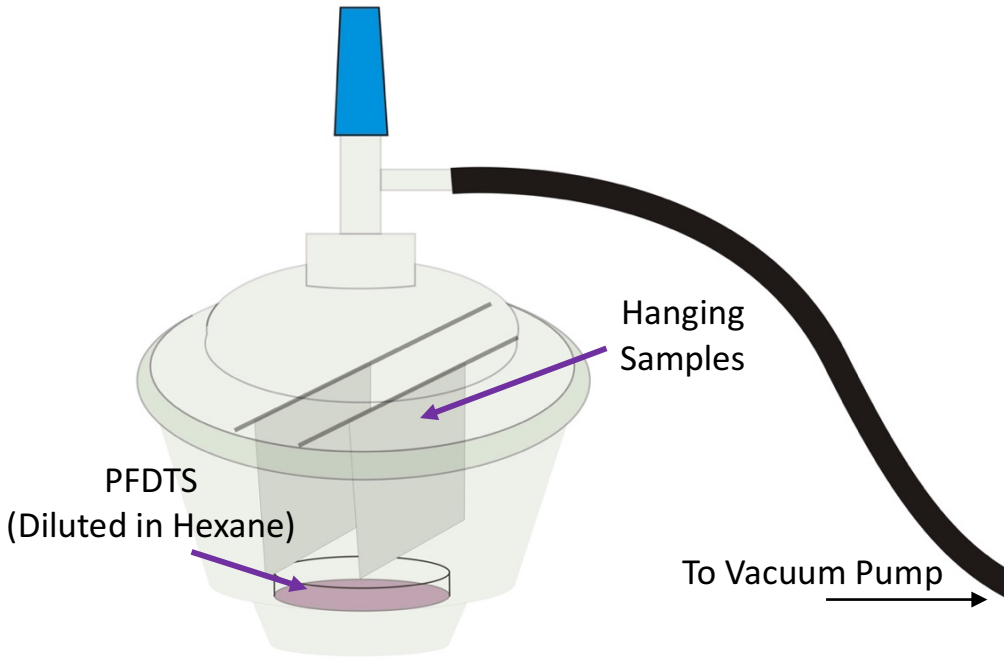

Table 3.1 Specimen codes

Code	Description
F	Untreated spin-coated film
F_{pl}	Film treated by air plasma
F_{vc}	Film treated by air plasma followed by PFDTS vapor coating
E	Untreated electrospun web
E_{pl}	Electrospun web treated by air plasma
E_{vc}	Electrospun web treated by air plasma followed by PFDTS vapor coating

Characterization of morphology and wetting properties

Contact angle measurement

The surface energy of pristine PS film (F), and PS films treated by the air plasma (F_{pl}), and PS films treated by PFDTS vapor deposition (F_{vc}) were analyzed by the Owens-Wendt method and Wu's method with the measured values of water contact angle and MI contact angle (Correia, Ramos, Saramago, & Calado, 1997). According to these two models, the surface energy of a smooth surface can be estimated by measuring the contact angles of two different liquids whose surface energy components are known. The surface energy components of water and MI (Żenkiewicz, 2007) are given in **Table 3.2**.

Table 3.2 Polar (δ_L^{Polar}) and disperse ($\delta_L^{Disperse}$) components of surface tension of water and methylene iodide (Żenkiewicz, 2007).

Chemical	δ_L^{Polar}	$\delta_L^{Disperse}$	γ_L
Water	51.0	21.8	72.8
Methylene iodide	0.0	50.8	50.8

**The unit of surface tension is mN/m.*

In the Owens-Wendt model (Owens & Wendt, 1969), for one phase condition (liquid or solid), surface free energy can be represented by the following equation:

$$\delta = \delta^{Disperse} + \delta^{Polar}.$$

At the solid-liquid interface, the interfacial tension (γ_{LS}) between the liquid and solid can be expressed as follows:

$$\gamma_{LS} = 2\left(\sqrt{\delta_L^{Disperse} \cdot \delta_S^{Disperse}} + \sqrt{\delta_L^{Polar} \cdot \delta_S^{Polar}}\right)$$

Using the Young's Equation (1) (Young, 1805), the interfacial tension between the liquid and solid, γ_{LS}, can be calculated by:

$$\gamma_{LS} = \frac{\gamma_L(1 + cos\theta^Y)}{2} \quad (1)$$

γ_L: surface tension of the liquid

θ^Y: static contact angle of liquid on a smooth solid surface

$\delta_L^{Disperse}$: disperse component of surface tension of liquid (known from reference)

δ_L^{Polar}: disperse component of surface tension of liquid (known from reference)

$\delta_S^{Disperse}$: disperse component of surface tension of solid (unknown, to be calculated)

δ_S^{Polar}: polar component of surface tension of solid (unknown, to be calculated).

With the measured contact angle of two different liquids on polystyrene surface, θ^Y, the polar component and the disperse component of the surface energy of solid can be estimated. In our study, we used water and MI as two different liquids, and their disperse and polar components of surface tension are known from literature (Żenkiewicz, 2007). The following shows the calculation of $\delta_S^{Disperse}$ and δ_S^{Polar}:

$$\frac{\gamma_L(1+cos\theta_{WA}^{Y})}{2} = 2\left(\sqrt{\delta_{WA}^{Disperse}\cdot\delta_S^{Disperse}} + \sqrt{\delta_{WA}^{Polar}\cdot\delta_S^{Polar}}\right) \quad (2)$$

$cos\theta_{WA}^{Y}$: static contact angle of water on a smooth surface (known by measurement)

$\delta_{WA}^{Disperse}$: disperse component of surface tension of liquid (known from reference)

δ_{WA}^{Polar}: polar component of surface tension of water (known from reference),

$$\frac{\gamma_L(1+cos\theta_{MI}^{Y})}{2} = 2\left(\sqrt{\delta_{MI}^{Disperse}\cdot\delta_S^{Disperse}} + \sqrt{\delta_{MI}^{Polar}\cdot\delta_S^{Polar}}\right) \quad (3)$$

$cos\theta_{MI}^{Y}$: static contact angle of MI on a smooth surface (known by measurement)

$\delta_{MI}^{Disperse}$: disperse component of surface tension of MI (known from reference)

δ_{MI}^{Polar}: polar component of surface tension of MI (known from reference).

Two unknown variables, disperse and polar components of the surface energy for a solid, $\delta_S^{Disperse}$ and δ_S^{Polar}, can be obtained by solving equations (2) and (3). Finally, the surface energy of solid surface, γ_s, is demonstrated by equation (4) in the following equation:

$$\gamma_s = \delta_s^{Disperse} + \delta_s^{Polar} \quad (4)$$

Instead of the geometric mean of a disperse part and a polar part of the surface tension or surface free energy in the Owens-Wendt model (Owens & Wendt, 1969), the interactions in the Wu's model (Wu, 1971) are interpreted as the harmonic mean of these two part as follows:

$$\gamma_{LS} = \gamma_L + \gamma_S - 4\left(\frac{\delta_L^{Disperse}\cdot\delta_s^{Disperse}}{\delta_L^{Disperse}+\delta_s^{Disperse}} + \frac{\delta_L^{Polar}\cdot\delta_S^{Polar}}{\delta_L^{Polar}+\delta_S^{Polar}}\right)$$

According to equation (1), the equation can be rewritten as follows:

$$\frac{\gamma_L(1+cos\theta^{Y})}{2} = \gamma_L + \gamma_S - 4\left(\frac{\delta_L^{Disperse}\cdot\delta_s^{Disperse}}{\delta_L^{Disperse}+\delta_s^{Disperse}} + \frac{\delta_L^{Polar}\cdot\delta_S^{Polar}}{\delta_L^{Polar}+\delta_S^{Polar}}\right) \quad (5)$$

where θ^{Y} refers to the static contact angle on a smooth surface.

With the measured contact angle of two liquids for polystyrene surfaces, the polar component and the disperse component of the surface energy can be estimated by Wu's method (Wu, 1971). Thus, the surface energy of the solid surface was obtained by combining equations (4) and (5). To this end, the polar and disperse parts were calculated by equations (6) and (7):

$$\frac{\gamma_L(1+cos\theta_{WA}^{Y})}{2} = \gamma_L + \gamma_S - 4\left(\frac{\delta_{WA}^{Disperse}\cdot\delta_s^{Disperse}}{\delta_{WA}^{Disperse}+\delta_s^{Disperse}} + \frac{\delta_{WA}^{Polar}\cdot\delta_S^{Polar}}{\delta_{WA}^{Polar}+\delta_S^{Polar}}\right) \quad (6)$$

$$\frac{\gamma_L(1+cos\theta_{MI}^{Y})}{2} = \gamma_L + \gamma_S - 4\left(\frac{\delta_{MI}^{Disperse}\cdot\delta_s^{Disperse}}{\delta_{MI}^{Disperse}+\delta_s^{Disperse}} + \frac{\delta_{MI}^{Polar}\cdot\delta_S^{Polar}}{\delta_{MI}^{Polar}+\delta_S^{Polar}}\right) \quad (7)$$

Microscopic analysis

The morphology and surface roughness of the PS films and the electrospun webs were observed by a field-emission scanning electron microscope (FE-SEM) (Versa 3D Dual Beam, FEI, USA). Prior to SEM analysis, all specimens were coated with an approximately 20 nm thick Au/Pd (gold palladium alloy) layer using a sputter coater (150TS, Quorum, UK). The SEM images for surface morphology and roughness structure, such as fiber diameter, beaded form, wrinkles and pores of fibers, were further analyzed by ImageJ software (version 1.46r, NIH, USA).

The theoretical solid fraction f_s of the Cassie-Baxter model was calculated using the contact angles measured from a rough surface (electrospun web) and a flat surface (spin coated film). The actual contact area between water and the PS electrospun web was observed by a laser scanning confocal microscope (LSM 5 Pascal, Zeiss) with a hydrophobic fluorescent dye, coumarin 314. The aqueous solution with coumarin dye was prepared in a concentration of 0.73 g/L (~ 5 mM). Although coumarin is a hydrophobic dye, a small amount is soluble in water (up to ~1.7 g/L). A drop of the dye solution was rolled on an electrospun web with a pipette and then removed from the surface (**Figure 3.3**). Due to the hydrophobic nature of coumarin, we assumed

that the hydrophobic PS surface was stained by coumarin when PS web was contacted by the aqueous coumarin solution. The surface area where coumarin adhered to was observed by a fluorescence microscope, and the area fraction of the fluoresced area (f_s^{dye}) was measured by ImageJ. For this analysis, at least four measurements of the fluorescence images per sample were used. This f_s^{dye} was regarded as the solid fraction where the water was actually in contact with. The f_s^{dye} was used to predict the apparent contact angle of the PS web, and the predicted CA was compared with the measured CA.

Figure 3.3 Process of staining method for the characterization of interfacial area between water and repellent surface.

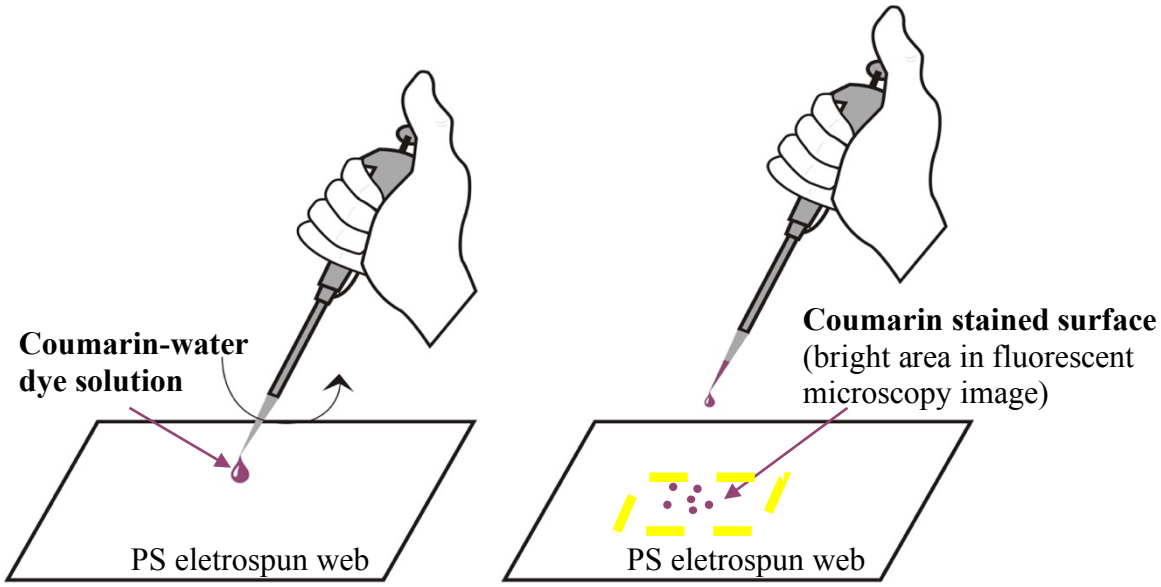

Step 1: Rolling the coumarin-water dye solution droplet on PS electrospun webs surface

Step 2: Suction of the coumarin-water solution droplet

Chapter 4 - Results and discussion

Influence of surface morphology on wettability

To investigate the influence of surface roughness on wettability, PS electrospun webs in different morphologies were produced by varying the conditions of a polymer solution, such as concentration of PS and solvent mixing ratio. It has been reported that a polymer solution in a mixture of solvents with different volatilities can create pores and corrugations (wrinkles) by phase separation (Kang et al., 2008; Lin et al., 2010). In our study, THF and DMF were employed as a volatile and a less-volatile solvent, respectively. SEM images of electrospun webs were observed for fiber morphology and surface roughness.

As shown in **Figure 4.1**, beaded structure becomes dominant at lower polymer concentrations, while fibrous structures become dominant at higher polymer concentrations, regardless of solvent mixing ratios. The polymer solution of 30% PS content only produced non-beaded fibers, while the morphology at 20% PS concentration was in transition between the beaded and fibrous structure. This morphological variation is attributed to the solution viscosity. When the viscosity of a solution is too low (at low concentrations), a jet collapses into droplets before the solvent evaporates, leading to bead formation (Frenot & Chronakis, 2003). When the viscosity or polymer concentration reaches the critical point where chain entanglement occurs, jet breakup is prevented so that uniform fibers can be produced (Gupta, Elkins, Long, & Wilkes, 2005). Above this critical polymer entanglement point, fibers become thicker and smoother as viscosity is increased (Sas et al. 2012). Thus, in addition to the effect of polymer concentration on the formation of beaded structure, low polymer concentration contributed to a smaller fiber diameter (**Table 4.1**). From the observations on morphological structure and fiber diameters with different polymer concentrations, hypothesis 1 was proven such that, *in electrospinning, higher*

concentrations (above the critical point for chain entanglement) of polymer solution will produce uniform fibers, while lower concentrations (below the critical point for chain entanglement) of polymer solution will produce beads.

Solvent volatility also affects the morphology of the web produced by the electrospinning process. Polymer dissolved in pure THF could not be electrospun as THF evaporated too quickly. The mixing ratio of THF: DMF was varied as 3:1, 2:2, 1:3, and 0:4 in this study and SEM images of the webs produced at those conditions are presented in **Figure 4.1**. A highly evaporative solvent reduces the time to solidify polymers, generally giving a coarse surface (Subbiah et al., 2005). Also, a mixture of solvents with different volatilities is reported to form pores or corrugations by phase separation. Phase separation occurs when a polymer solution separates into polymer-rich and solvent-rich regions, as one of the solvents evaporates more quickly than the other, forming pores and irregularities on the surface (Qi, Yu, Chen, & Zhu, 2009; Subbiah et al., 2005). With a higher ratio of DMF (THF: DMF of 0:4 and 1:3), fine pores were formed on the surface of beads and fibers. These fine pores could also be caused by the adsorption of water vapor from the atmosphere (45±5 %RH), leaving an imprint of fine pores after water molecules evaporate (Qi et al., 2009).

As the ratio of THF increases (3:1 THF: DMF), the surface of the beads or fibers became more corrugated or wrinkled. In this case, more volatile THF evaporates more quickly and solidifies at the skin of the fiber, and softer core loses the capability to support the skin, finally collapsing and forming a wrinkled structure (Katsogiannis, Vladisavljević, & Georgiadou, 2015). By comparing the fiber morphologies produced at different mixing ratio of solvents, the results proved hypothesis 2, *a mixture of solvents with different volatilities will generate irregular surface morphology during electrospinning*.

Table 4.1 Fiber diameters of PS electrospun webs with different polymer concentration and solvent mixture ratio.

Solvent mixture ratio (THF:DMF)		0:4	1:3	2:2	3:1
		Fiber diameters (SD)			
Concentration	10%	0.18 (±0.06)	0.25 (±0.08)	1.11 (±0.42)	0.15 (±0.05)
	20%	1.69 (±0.38)	2.72 (±0.27)	4.15(±0.85)	4.79 (±1.99)
	30%	3.27 (±0.40)	4.21 (±0.60)	4.35(±0.30)	5.05 (±0.58)

** All units of fiber diameters are μm.*
** 30 PS fibers were randomly selected in one random SEM image for measuring the average and standard deviation of the fiber diameters.*

From the various PS fiber morphologies produced by different electrospinning conditions, the surface roughness of PS webs was also varied. In order to evaluate the relationship between the PS fiber morphology (roughness) and wettability, water contact angle (CA) on the electrospun webs was measured (**Figure 4.1**). CA on the flat PS film surface was 95˚; compared to the CA on the flat surface, CAs on the electrospun webs were considerably increased (139˚~161˚) due to the increased surface roughness by fine fibers and beads on the web. According to the Wenzel (Wenzel, 1936) and the Cassie-Baxter (Cassie &Baxter, 1944) theories, for the flat surface of which CA is higher than 90˚, the wettability is further lowered when surface roughness is introduced. From the comparison of CAs on flat film and roughened webs, hypothesis 3, *increased roughness on a hydrophobic surface will enhance anti-wettability,* was proven.

Figure 4.1 Morphology of the PS electrospun webs produced from different conditions: water contact angle (CA) is presented by the mean value and standard deviation (SD).

10% PS	THF:DMF (Voltage)	0:4 (10.5 kV)	1:3 (9.5 kV)	2:2 (9 kV)	3:1 (7 kV)
	CA ˚ (SD)	156˚ (±2.7)	151˚ (±2.3)	153˚ (±1.9)	161˚ (±2.7)
	SEM Image	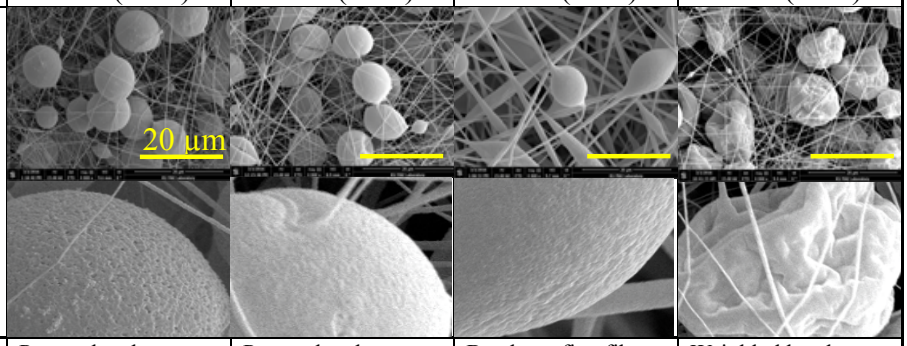			
	Morphology	Porous beads on fine fibers	Porous beads on fine fibers	Beads on fine fibers	Wrinkled beads on fine fibers
20% PS	THF:DMF (Voltage)	0:4 (14 kV)	1:3 (14 kV)	2:2 (14 kV)	3:1 (14 kV)
	CA ˚ (SD)	147˚ (±3.9)	153˚ (±3.2)	148˚ (±1.9)	155˚ (±2.1)
	SEM image	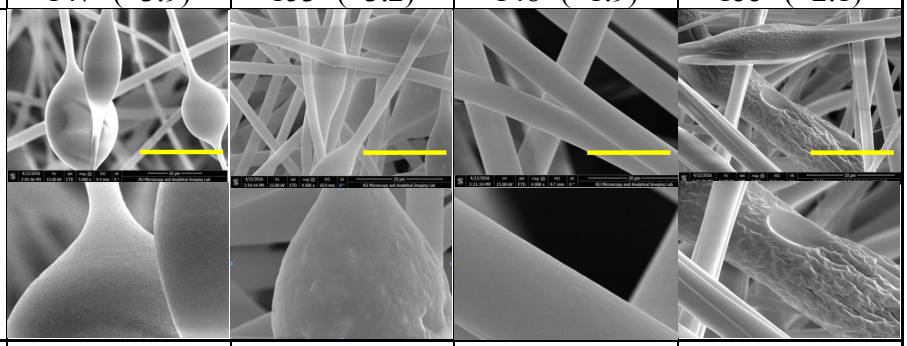			
	Morphology	Beaded fibers	Beaded fibers	Smooth fibers	Wrinkled fibers
30% PS	THF:DMF (Voltage)	0:4 (14 kV)	1:3 (14 kV)	2:2 (14 kV)	3:1 (14 kV)
	CA ˚ (SD)	139˚ (±2.7)	142˚ (±2.2)	144˚ (±2.5)	155˚ (±2.1)
	SEM Image	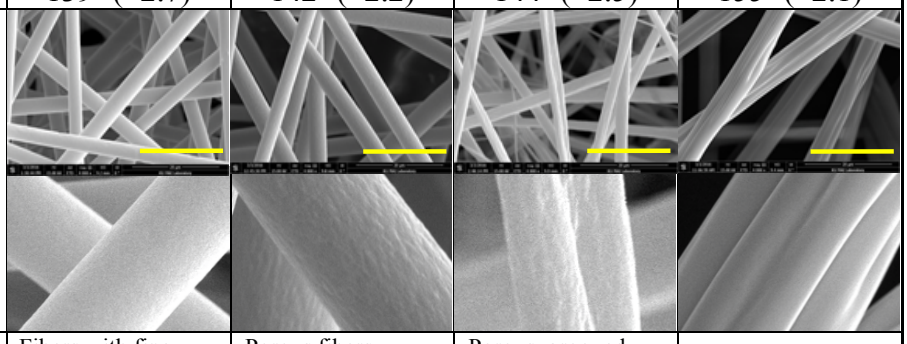			
	Morphology	Fibers with fine pores	Porous fibers	Porous, grooved fibers	Grooved fibers

** All inserted yellow bar represents a length of 20 µm.*

** The lower images in each sections are enlarged in random magnifications to show the surface patterns.*

Among the web morphologies, beaded structures tend to produce higher CAs (147˚~161˚) than the uniform fibers (139˚~155˚), probably due to the increased roughness contributed by the "secondary roughness" onto a fibrous web (Megelski et al., 2002). The wrinkled beads on fine fiber structures presented the highest hydrophobicity (CA=161˚) among the webs. CAs on the webs with relatively smooth beads and porous beads ranged 147˚~156˚. Also, grooved fibers presented higher hydrophobicity (CA=155˚) than smooth fibers (148˚) and porous fibers (139˚~144˚), which is similar to the findings from previous studies (Miyauchi et al., 2006; Zheng et al., 2006).

Modification of surface energy

In order to further investigate the combined effect of surface roughness and surface energy, PS film (F) and electrospun webs (E) were subjected to the chemical modifications to change the surface energy. To increase the surface energy, substrates were treated by air plasma, which led to surface oxidation. To decrease the surface energy, plasma-treated PS substrates were subjected to the chemical vapor deposition of PFDTS. Chemical compositions of the untreated PS and the modified PS surfaces were analyzed by FTIR (**Figure 4.2**). Bands of the FTIR spectrum for PS correspond to their aliphatic and aromatic C-H stretching in 2850 cm^{-1} ~3100 cm^{-1}. The bands in this region appear commonly for all the tested PS surfaces. After plasma treatment, bands in 1100 cm^{-1}~1300 cm^{-1} appear, which correspond to C-O functional group. With the subsequent PFDTS vapor coating, the bands in 1000 cm-^{1}~1300 cm^{-1} appear, which might come from the C-F stretching (PFDTS itself) and the chemical bonding between PS and PFDTS (Si-O-C stretching and Si-CH_3 bending). The peaks in spectra corroborate the presence of functional groups that were introduced by the surface oxidation (by air plasma) and the hydrophobization (by PFDTS vapor coating).

Figure 4.2 FTIR spectra of PS substrates

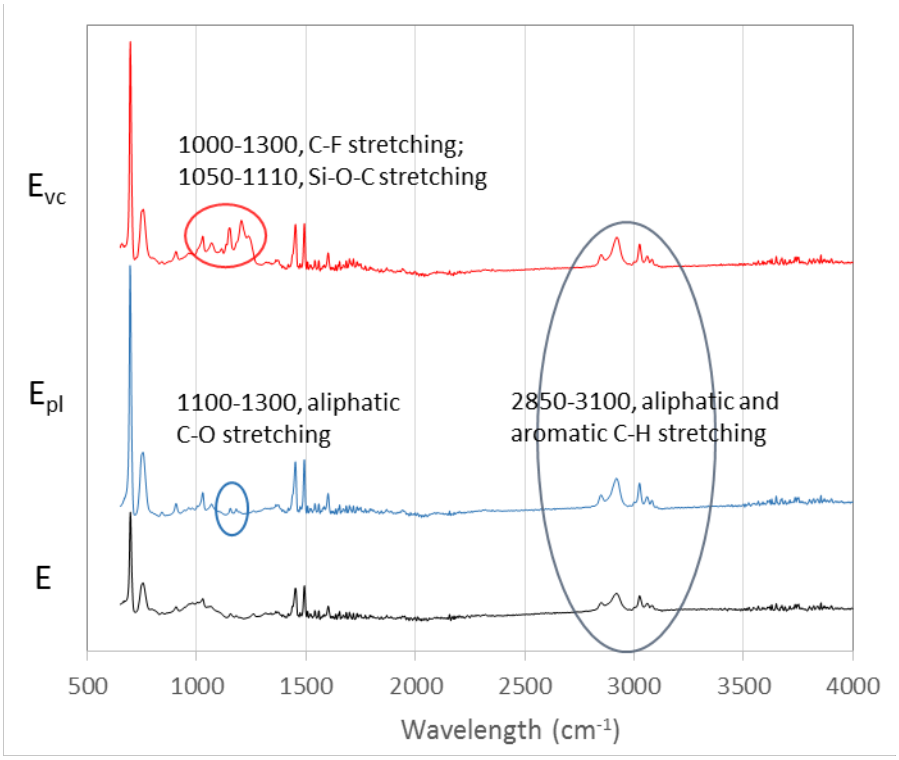

(a) untreated PS electrospun web, E; (b) PS web treated by air plasma, E_{pl}; (c) PS web treated by air plasma followed by PFDTS vapor coating, E_{vc}.

The FTIR results indicated that surface chemistry (chemical bonds or surface functional groups) was changed after these surface chemical modifications. With the modification of surface chemistry, the surface energy (SE) of the PS substrates was changed. In order to prove the change of surface energy of PS surfaces after surface modification, the surface energy value was estimated using both the Wu's method (Wu, 1971) and the Owens-Wendt method (Owens & Wendt, 1969) by measuring the CAs of water (WA) and methylene iodide (MI) on flat PS surfaces (F, F_{pl}, and F_{vc}). The estimated surface energy components of the F, F_{pl}, and F_{vc} are presented in **Table 4.2** along with the CAs of WA and MI. The surface energies estimated by two methods are different, because the Wu's method (Wu, 1971) employs the harmonic mean of dispersive and polar components of surface energy whereas the Owens-Wendt method (Owens &

Wendt, 1969) uses the geometric mean of those components. The Wu's method (Wu, 1971) is commonly used to estimate the surface energy lower than 40 mN/m, while the Owens-Wendt method (Owens & Wendt, 1969) is adopted as a standard method in general (Kim et al., 2015). The estimates by both methods are presented in **Table 4.2**.

Table 4.2 Contact angle of water and methylene iodide, and surface energy estimated by Wu's (Wu, 1971) and Owens-Wendt (Owens & Wendt, 1969) models

Specimen	Contact angle (˚)		Surface energy by the Wu's method (mN/m)			Surface energy by the Owens-Wendt' method (mN/m)		
	WA	MI	γ_S	γ^d_S	γ^p_S	γ_S	γ^d_S	γ^p_S
F	95˚	39˚	43.2	40.6	2.6	40.4	40.1	0.3
F_{pl}	21˚	18˚	81.7	48.4	33.3	76.5	48.3	28.2
F_{vc}	115˚	99˚	15.8	13.6	2.2	10.0	9.0	1.0

** γ_S, surface energy of PS; γ^d_S, dispersive component of surface energy of PS; γ^p_S, polar component of surface energy; γ_L, surface tension of liquid; γ^d_L, dispersive component of surface tension of liquid; γ^p_S, polar component of surface tension of liquid.*

** For water, γ_L 72.8 mN/m; γ^d_L 21.8 mN/m; γ^p_S 51.0 mN/m (Żenkiewicz, 2007).*

** For MI, γ_L 50.8 mN/m; γ^d_L 50.8 mN/m; γ^p_S 0 mN/m(Żenkiewicz, 2007).*

Compared to the untreated PS substrate (SE: 40.4~43.2 mN/m), the surface energy of the plasma treated substrate was considerably increased to 75.5~81.7 mN/m. With the PFDTS coating, the surface energy was significantly reduced to 10.0~15.8 mN/m (the value varies depending on the estimation method). According to the manufacturer's specification, the surface energy of PFDTS was 17.2 mN/m. Previously it was reported that the surface energy of a homogeneous, dense layer of PFDTS with CF_3 terminal groups assembled on a surface can reach down to 6 mN/m (Brzoska, Azouz, & Rondelez, 1994). The surface energy of the PFDTS treated specimen in this study lied between the values from a previous study (6 mN/m) and the manufacturer's specification of PFDTS (17.2 mN/m).

Both the FTIR results of PS electrospun webs and the value of surface energy of F, F_{pl}, and F_{vc} provided the evidence that surface energy was increased by air plasma treatment and decreased by PFDTS vapor deposition.

Combined effect of surface energy and morphology on wettability

Among the webs presented in **Figure 4.2**, three webs in a high CA range (10%-0:4, 10%-3:1, 30%-3:1), one web with the lowest CA (30%-0:4), and one web in between (30%-1:3) were selected for surface modifications, and further analysis was performed to examine the effects of surface modification on the wettability (**Table 4.3**). When the surface was treated by air plasma, all electrospun webs (ES) were completely wet. With PFDTS coating, E_{vc} exhibited superhydrophobic property (water CA > 150˚) and super-repellent property (water CA > 150˚ and water SA<10˚), while F_{vc} did not reach that level of superhydrophobicity (CA~115˚). From this result, it appears that there are limitations in achieving a superhydrophobic/super-repellent surface solely by lowering the surface energy, and surface roughness can have a substantial impact on anti-wettability. Although some PS electrospun webs (E) achieved superhydrophobicity with the water contact angle over 150˚, a droplet did not roll off from the surface at a small tilted angle; however, the E_{vc} showed roll-off of droplets at low sliding angles (SA) and achieved super-repellency.

The air plasma treated film (F_{pl}) had lower contact angle (21˚) than the pristine film (F) due to the increased surface energy. According to the Young's model (Young, 1805), higher surface energy contributes to a lower contact angle on a flat surface. Compared to the plasma-treated PS film (F_{pl}), the plasma-treated PS electrospun webs (E_{pl}) presented higher wettability (completely wet) due to the combined effect of increased surface energy and existence of surface roughness; on the other hand, the PFDTS vapor coated PS electrospun webs (E_{vc}) presented

higher level of anti-wettability or super-repellency than the PFDTS coated PS film (F_{vc}) due to the combined effect of lowered surface energy and existence of roughness. According to these results, it was concluded that implementation of surface roughness can amplify the wettability or anti-wettability, depending on the surface energy of materials, thereby proving the following hypotheses 3 and 4:

Hypothesis 3: increased roughness on a hydrophobic surface will enhance anti-wettability.

Hypothesis 4: increased roughness on a hydrophilic surface will enhance the wettability.

When surface roughness is introduced to a low surface energy material, liquid is in contact with both the solid surface and the air pockets present between rough bumps, exhibiting the Cassie-Baxter state (Cassie & Baxiter, 1944). At the Cassie-Baxter state, the contact area between the liquid drop and solid surface is reduced, and the adhesion between them is weakened, allowing easy roll-off of droplets. On the contrary, in the Wenzel's state (Wenzel, 1936), liquid is in contact solely with the solid surface (without air pocket), and the contact area of the liquid at the roughened surface is higher than that at the flat surface. Thus, in the Wenzel's state (Wenzel, 1936), although the surface shows superhydrophobicity with an above 150˚ WCA, higher energy is required to cause a liquid drop to be separated from the solid surface, making roll-off difficult (Nishimoto & Bhushan, 2013). The ability of roll-off is commonly evaluated by the sliding angle (SA) measurement (Sas et al., 2010); a lower sliding angle represents easier roll-off and higher repellency.

On F_{vc} surface, a water drop did not roll-off easily, and SA was not measurable. However, E_{vc} surfaces with beads and corrugated fibers exhibited low SAs (3˚~3.5˚). E_{vc} surfaces with smooth fibers showed SAs of 9˚~11˚ (**Table 4.3**). From the SA measurements, it is

speculated that the additional surface patterns such as beads and corrugations are beneficial to reduce the contact area between water and solid, leading to the Cassie-Baxter (Cassie & Baxiter, 1944) wetting state. On E_{vc} surfaces with beads and grooved fibers a water drop rolled off at a low sliding angle, which is an indication of self-cleaning performance due to the combined effect of low surface energy and the roughened morphology. Though the produced nonwoven material exhibited the limited mechanical durability, such materials with highly repellent property will have potential applications in air filtration, liquid separation, disposable personal protective equipment.

Table 4.3 Water contact angle (CA) and sliding angle (SA) of PS substrates with different surface modifications.

	Film (F)	Electrospun webs (ES)				
PS conc. % (w/w)	12%	10%		30%		
THF:DMF	Toluene	1:3	3:1	0:4	1:3	3:1
SEM image	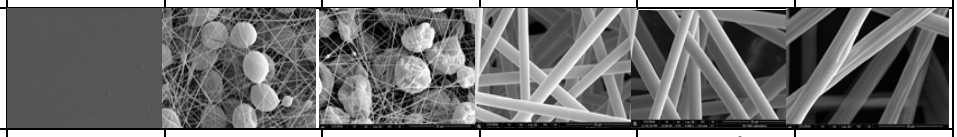					
CA untreated	95˚ (±1.1)	151˚ (±2.3)	161˚ (±2.6)	139˚ (±2.7)	142˚ (±2.2)	155˚ (±2.1)
CA plasma-treated	21˚ (±1.4)	0˚ (all specimens were completely wet)				
CA vapor coated	115˚ (±1.6)	171˚ (±2.5)	172˚ (±2.0)	163˚ (±1.5)	159˚ (±4.8)	169˚ (±3.5)
SA vapor coated	N/A	3.5˚ (±0.5)	3˚ (±0.3)	9˚ (±1.8)	11˚ (±1.0)	3˚ (±0.5)

Analysis of solid fraction and prediction of wettability

The solid area fraction refers to the proportion of the area where water and solid surface are in contact in the Cassie-Baxter wetting state (Cassie & Baxter, 1944). The Cassie-Baxter equation (Cassie & Baxter, 1944) explains the relationship between *fs* (solid area fraction),

θ^Y(Young's WCA at a flat surface), and θ^C(the apparent WCA in Cassie-Baxter's wetting state) as follows:

$$\cos\theta^C = f_s(\cos\theta^Y + 1) - 1$$

The calculation of solid fraction f_s is based on the Cassie-Baxter's assumption that a water drop is in contact with only the upper area of the roughened surface, leaving the air pockets unwet. This assumption would be valid when a liquid with high surface tension is placed on a super-repellent surface without penetrating into the pores and roughened structures. By visually observing where water is actually in contact with on a roughened repellent surface, an actual solid area fraction was measured to compare it with the theoretical f_s value predicted from the Cassie-Baxter model (Cassie & Baxter, 1944).

In order to investigate the actual solid fraction where the water is in contact with, a simple characterization method was developed in this study. In this method, an aqueous solution with a hydrophobic fluorescent dye, coumarin, was prepared. Though coumarin is a hydrophobic dye, a small amount of it can be dissolved in water. As coumarin is hydrophobic, it was anticipated that coumarin has more affinity to hydrophobic PS than water. It was observed that coumarin dye stained the contacted PS web surface when a drop of coumarin/water solution was rolled on the web. The fluoresced area by coumarin staining was observed by fluorescence microscopy. The fraction of the fluoresced area from the image, f_s^{dye}, was measured by ImageJ and was regarded as the actual solid fraction contacted by water. For the analysis of solid fraction f_s in the Cassie-Baxter model (Cassie & Baxter, 1944), three most anti-wetting surfaces were chosen among the tested samples, including untreated (E) and vapor coated (E_{vc}) webs.

In **Figure 4.3**, the solid fraction f_s^{dye} that was visually observed by fluorescence microscopy is presented, with the predicted water contact angle (WCA) from this f_s^{dye} value. In

order to evaluate the validity of this developed method for direct observation of the contact area between the water and repellent surface, the f_s^{dye} was compared with the solid fraction *fs* that was theoretically estimated by the Cassie-Baxter model (Cassie & Baxter, 1944). Also, the predicted WCA was compared with the measured WCA on the repellent PS web.

For E_{vc} surfaces that showed super-repellent characteristics, f_s^{dye} and the predicted CAs corresponded fairly well with the theoretical *fs* and the measured CAs, respectively. The prediction of WCA was more accurate for the super-repellent samples (E_{vc} samples) than the superhydrophobic samples (E samples). As E_{vc} samples (CA≥169°, SA≤3.5°) are more repellent than E samples, the surfaces of E_{vc} would fit more closely with the Cassie-Baxter wetting state (Cassie & Baxter, 1944; Sas et al., 2012), resulting in more accurate predictions. The WCAs of the untreated electrospun webs were not as high as those of the vapor coated webs, and the superhydrophobic untreated webs did not have the repellency with high roll-off angles; thus, their wetting state might be in transition between the Wenzel and the Cassie-Baxter states (Sas et al., 2012), in which the liquid is partially penetrated through the rough structures. It is also possible that the dye has not fully adhered to its contacted surface, underestimating the solid fraction especially for the highly repellent surfaces. Thus, an appropriate selection of a dye will be necessary.

The proposed characterization method will be useful to estimate the solid fraction and the apparent contact angle for the interface that follows the Cassie-Baxter state. However, this method gives only two-dimensional measurements. If a method that allows to measure a three-dimensional interface can be developed, it will be useful for predicting the wettability that may not follow the Cassie-Baxter wetting state.

Figure 4.3 Fluorescent images for PS surfaces to which coumarin dye adhered

PS % (THF:DMF)	10% (3:1)	30% (0:4)	30% (3:1)
Untreated electrospun web (E)			
Fluorescence microscopy	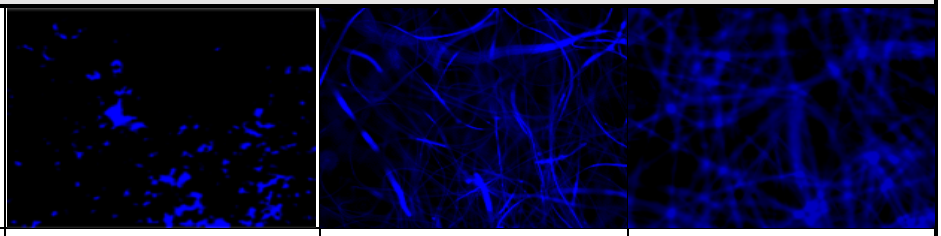		
Theoretical *fs*	0.060	0.269	0.103
fs^{dye}: measured from fluorescence area	0.060~0.073	0.199~0.307	0.095~0.178
Measured WCA	161˚ (±2.6)	139˚ (±2.7)	155˚ (±2.1)
Predicted WCA using fs^{dye}	159˚~161˚	136˚~145˚	147˚~156˚
Vapor coated electrospun web (E_{vc})			
Fluorescence microscopy	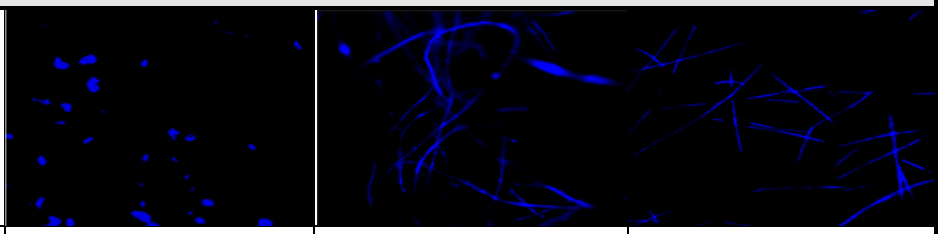		
Theoretical *fs*	0.017	0.076	0.032
fs^{dye}: measured from fluorescence area	0.015~0.032	0.068~0.078	0.029~0.036
Measured WCA	172˚ (±2.0)	163˚ (±1.5)	169˚ (±3.5)
Predicted WCA using fs^{dye}	169˚~172˚	163˚~164˚	168˚~170˚

∗Theoretical fs was calculated from Cassie-Baxter equation (Cassie & Baxter, 1944) by using measured WCA on flat PS film and electrospun web.

∗Solid area fraction fs^{dye} measured by staining method, equals to the bright fluorescence area in the image/whole area of the image.

∗Predicted WCA on PS electrospun web was calculated by measured solid area fraction and WCA measure on flat PS film.

Conclusion

Superhydrophobic/super-repellent PS webs in different surface morphologies were produced via the electrospinning and vapor coating processes. At low concentrations of the polymer solution (~10 %), beads were dominant, while fibrous forms were dominant at high polymer concentrations (~30 %). In a mixed solvent system with THF and DMF, the surface had pores or corrugations due to the phase separation of polymer-rich and solvent-rich regions (Katsogiannis, Vladisavljevic & Georgiadou, 2015).

Compared to a flat film (CA~95˚), the electrospun webs (CA>139˚) showed higher anti-wettability due to the surface roughness created by fibers and beads. Surface energy was modified to increase (75~82 mN/m) and to decrease (10~16 mN/m) by air-plasma and PFDTS coating, respectively. With the PFDTS coating, the electrospun webs (E_{vc}) exhibited superhydrophobicity with CA≥169˚, while CA of the PFDTS coated film (F_{vc}) was 115˚. From this result, it can be concluded that there is limitation in achieving superhydrophobic surface solely by lowering the surface energy, and surface roughness has a substantial impact on achieving the anti-wettability. E_{vc} also exhibited super-repellency with low SAs (≤3.5˚), implying that the introduced roughness reduced the contact area between the water and the solid surface, leading to the Cassie-Baxter (Cassie & Baxter, 1944) wetting state. Since the produced material was too weak for practical applications, future work is recommended to fabricate the mechanically durable superhydrophobic materials that can be used in practical end use. In this study, the repellency of material was tested only with water, whose surface tension is relatively high. It is, therefore, recommended to test the materials' repellency against various liquids of which surface tensions are lower and test the materials' potential application as protective layers to hazardous liquids.

The solid area fraction is used to describe the interfacial area between water and the solid surface in wetting models. In this study, the theoretical solid fraction of the Cassie-Baxter equation, f_s, was calculated from the CAs measured on the rough and flat surfaces. This theoretical f_s was compared with the solid fraction that was visually observed (f_s^{dye}) by tracing the hydrophobic fluorescence dye in water drops. The measured f_s^{dye} and the predicted WCA by this measured solid area fraction value corresponded fairly well with the actual measurement of WCA, especially for E_{vc}, of which surface appears to follow the Cassie-Baxter wetting state (Cassie & Baxter, 1944). The good correspondence between the theoretical and measured values shows the validity of the staining method for visually presenting the actually wetted area on the repellent surface. Future study is recommended to develop an advanced characterization method that enables the visualization of a wet surface in three dimensions to predict the wettability in various wetting states.

References

Aulin, C., Netrval, J., Wågberg, L., & Lindström, T. (2010). Aerogels from nanofibrillated cellulose with tunable oleophobicity. *Soft Matter*, 6(14), 3298-3305.

Bognitzki, M., Czado, W., Frese, T., Schaper, A., Hellwig, M., Steinhart, M., Greiner, A., Wendorff, J. H. (2001). Nanostructured fibers via electrospinning. *Advanced Materials*, 13(1), 70-72.

Borcia, G., Anderson, C. A., & Brown, N. (2004). The surface oxidation of selected polymers using an atmospheric pressure air dielectric barrier discharge. part II. *Applied Surface Science*, 225(1), 186-197.

Brzoska, J. B., Azouz, I. B., & Rondelez, F. (1994). Silanization of solid substrates: A step toward reproducibility. *Langmuir*, 10(11), 4367-4373.

Casper, C. L., Stephens, J. S., Tassi, N. G., Chase, D. B., & Rabolt, J. F. (2004). Controlling surface morphology of electrospun polystyrene fibers: effect of humidity and molecular weight in the electrospinning process. *Macromolecules*, 37(2), 573-578.

Cassie, A., & Baxter, S. (1944). Wettability of porous surfaces. *Transactions of the Faraday Society*, 40, 546-551.

Correia, N. T., Ramos, J. J. M., Saramago, B. J., & Calado, J. C. (1997). Estimation of the surface tension of a solid: Application to a liquid crystalline polymer. *Journal of Colloid and Interface Science*, 189(2), 361-369.

Ding, B., Li, C., Hotta, Y., Kim, J., Kuwaki, O., & Shiratori, S. (2006). Conversion of an electrospun nanofibrous cellulose acetate mat from a super-hydrophilic to super-hydrophobic surface. *Nanotechnology*, 17(17), 4332.

Doshi, J., & Reneker, D. H. (1993). Electrospinning process and applications of electrospun fibers. Paper presented at the *Industry Applications Society Annual Meeting*, 1993, *Conference Record of the 1993 IEEE*, 1698-1703.

Fong, H., Chun, I., & Reneker, D. H. (1999). Beaded nanofibers formed during electrospinning. *Polymer*, 40(16), 4585-4592.

Frenot, A., & Chronakis, I. S. (2003). Polymer nanofibers assembled by electrospinning. *Current Opinion in Colloid & Interface Science*, 8(1), 64-75.

Gupta, P., Elkins, C., Long, T. E., & Wilkes, G. L. (2005). Electrospinning of linear homopolymers of poly (methyl methacrylate): exploring relationships between fiber formation, viscosity, molecular weight and concentration in a good solvent. *Polymer*, 46(13), 4799-4810.

Huang, X., Wen, X., Cheng, J., & Yang, Z. (2012). Sticky superhydrophobic filter paper developed by dip-coating of fluorinated waterborne epoxy emulsion. *Applied Surface Science*, 258(22), 8739-8746.

Huang, Z., Zhang, Y., Kotaki, M., & Ramakrishna, S. (2003). A review on polymer nanofibers by electrospinning and their applications in nanocomposites. *Composites Science and Technology*, 63(15), 2223-2253.

Jarusuwannapoom, T., Hongrojjanawiwat, W., Jitjaicham, S., Wannatong, L., Nithitanakul, M., Pattamaprom, C., Koombhongse, P., Rangkupan, R., Supaphol, P. (2005). Effect of solvents on electro-spinnability of polystyrene solutions and morphological appearance of resulting electrospun polystyrene fibers. *European Polymer Journal*, 41(3), 409-421.

Kang, M., Jung, R., Kim, H., & Jin, H. (2008). Preparation of superhydrophobic polystyrene membranes by electrospinning. *Colloids and Surfaces A: Physicochemical and Engineering Aspects*, 313, 411-414.

Katsogiannis, K. A. G., Vladisavljević, G. T., & Georgiadou, S. (2015). Porous electrospun polycaprolactone (PCL) fibres by phase separation. *European Polymer Journal*, 69, 284-295.

Kim, J., Kim, H., & Park, C. H. (2016). Contribution of surface energy and roughness to the wettability of polyamide 6 and polypropylene film in the plasma-induced process. *Textile Research Journal*, 86(5), 461-471.

Kota, A. K., Kwon, G., & Tuteja, A. (2014). The design and applications of superomniphobic surfaces. *NPG Asia Materials*, 6(7), e109.

Kwon, S., Ko, T., Yu, E., Kim, J., Moon, M., & Park, C. H. (2014). Nanostructured self-cleaning lyocell fabrics with asymmetric wettability and moisture absorbency (part I). *RSC Advances*, 4(85), 45442-45448.

Leroux, F., Campagne, C., Perwuelz, A., & Gengembre, L. (2009). Atmospheric air plasma treatment of polyester textile materials. textile structure influence on surface oxidation and silicon resin adhesion. *Surface and Coatings Technology*, 203(20), 3178-3183.

Lin, J., Ding, B., & Yu, J. (2010). Direct fabrication of highly nanoporous polystyrene fibers via electrospinning. *ACS Applied Materials & Interfaces*, 2(2), 521-528.

Megelski, S., Stephens, J. S., Chase, D. B., & Rabolt, J. F. (2002). Micro-and nanostructured surface morphology on electrospun polymer fibers. *Macromolecules*, 35(22), 8456-8466.

Miwa, M., Nakajima, A., Fujishima, A., Hashimoto, K., & Watanabe, T. (2000). Effects of the surface roughness on sliding angles of water droplets on superhydrophobic surfaces. *Langmuir*, 16(13), 5754-5760.

Miyauchi, Y., Ding, B., & Shiratori, S. (2006). Fabrication of a silver-ragwort-leaf-like super-hydrophobic micro/nanoporous fibrous mat surface by electrospinning. *Nanotechnology*, 17(20), 5151.

Neinhuis, C., & Barthlott, W. (1997). Characterization and distribution of water-repellent, self-cleaning plant surfaces. *Annals of Botany*, 79(6), 667-677.

Nishimoto, S., & Bhushan, B. (2013). Bioinspired self-cleaning surfaces with superhydrophobicity, superoleophobicity, and superhydrophilicity. *RSC Advances*, 3(3), 671-690.

Owens, D. K., & Wendt, R. C. (1969). Estimation of the surface free energy of polymers. *Journal of Applied Polymer Science*, 13(8), 1741-1747.

Pan, Z., Shahsavan, H., Zhang, W., Yang, F. K., & Zhao, B. (2015). Superhydro-oleophobic bio-inspired polydimethylsiloxane micropillared surface via FDTS coating/blending approaches. *Applied Surface Science*, 324, 612-620.

Park, Y., Park, C. H., & Kim, J. (2014). A quantitative analysis on the surface roughness and the level of hydrophobicity for superhydrophobic ZnO nanorods grown textiles. *Textile Research Journal*, 84(16), 1776-1788.

Qi, Z., Yu, H., Chen, Y., & Zhu, M. (2009). Highly porous fibers prepared by electrospinning a ternary system of nonsolvent/solvent/poly (l-lactic acid). *Materials Letters*, 63(3), 415-418.

Reneker, D. H., & Chun, I. (1996). Nanometre diameter fibres of polymer, produced by electrospinning. *Nanotechnology*, 7(3), 216.

Sas, I., Gorga, R. E., Joines, J. A., & Thoney, K. A. (2012). Literature review on superhydrophobic self- cleaning surfaces produced by electrospinning. *Journal of Polymer Science Part B: Polymer Physics*, 50(12), 824-845.

Shafrin, E. G., & Zisman, W. A. (1960). Constitutive relations in the wetting of low energy surfaces and the theory of the retraction method of preparing monolayers[1]. *The Journal of Physical Chemistry*, 64(5), 519-524.

Shin, B., Lee, K., Moon, M., & Kim, H. (2012). Extreme water repellency of nanostructured low-surface-energy non-woven fabrics. *Soft Matter*, 8(6), 1817-1823.

Subbiah, T., Bhat, G. S., Tock, R. W., Parameswaran, S., & Ramkumar, S. S. (2005). Electrospinning of nanofibers. *Journal of Applied Polymer Science*, 96(2), 557-569.

Teare, D., Spanos, C. G., Ridley, P., Kinmond, E. J., Roucoules, V., Badyal, J. P. S., Brewer, S. A., Coulson, S., Willis, C. (2002). Pulsed plasma deposition of super-hydrophobic nanospheres. *Chemistry of Materials*, 14(11), 4566-4571.

Wang, S., & Jiang, L. (2007). Definition of superhydrophobic states. *Advanced Materials*, 19(21), 3423-3424.

Wenzel, R. N. (1936). Resistance of solid surfaces to wetting by water. *Industrial & Engineering Chemistry*, 28(8), 988-994.

Wolfs, M., Darmanin, T., & Guittard, F. (2013). Superhydrophobic fibrous polymers. *Polymer Reviews*, 53(3), 460-505.

Woodward, I., Schofield, W., Roucoules, V., & Badyal, J. (2003). Super-hydrophobic surfaces produced by plasma fluorination of polybutadiene films. *Langmuir*, 19(8), 3432-3438.

Wu, S. (1971). Calculation of interfacial tension in polymer systems. Paper presented at the *Journal of Polymer Science Part C: Polymer Symposia*, 34(1), 19-30.

Xue, C., Jia, S., Zhang, J., & Tian, L. (2009). Superhydrophobic surfaces on cotton textiles by complex coating of silica nanoparticles and hydrophobization. *Thin Solid Films*, 517(16), 4593-4598.

Xue, C., Li, Y., Zhang, P., Ma, J., & Jia, S. (2014). Washable and wear-resistant superhydrophobic surfaces with self-cleaning property by chemical etching of fibers and hydrophobization. *ACS Applied Materials & Interfaces*, 6(13), 10153-10161.

Yoon, Y. I., Moon, H. S., Lyoo, W. S., Lee, T. S., & Park, W. H. (2009). Superhydrophobicity of cellulose triacetate fibrous mats produced by electrospinning and plasma treatment. *Carbohydrate Polymers*, 75(2), 246-250.

Young, T. (1805). An essay on the cohesion of fluids. *Philosophical Transactions of the Royal Society of London*, 95, 65-87.

Żenkiewicz, M. (2007). Methods for the calculation of surface free energy of solids. *Journal of Achievements in Materials and Manufacturing Engineering*, 24(1), 137-145.

Zheng, J., He, A., Li, J., Xu, J., & Han, C. C. (2006). Studies on the controlled morphology and wettability of polystyrene surfaces by electrospinning or electrospraying. *Polymer*, 47(20), 7095-7102.

Zhu, M., Zuo, W., Yu, H., Yang, W., & Chen, Y. (2006). Superhydrophobic surface directly created by electrospinning based on hydrophilic material. *Journal of Materials Science*, 41(12), 3793-3797.